PRINTED TATTOO ELECTRODES FOR ELECTROPHYSIOLOGICAL SIGNAL ACQUISITION

YOLAND EL-HAJJ

A THESIS SUBMITTED TO THE FACULTY OF GRADUATE STUDIES
IN PARTIAL FULFILLMENT OF THE REQUIREMENTS FOR THE
DEGREE OF MASTER OF APPLIED SCIENCE

GRADUATE PROGRAMME IN ELECTRICAL ENGINEERING AND
COMPUTER SCIENCE YORK UNIVERSITY TORONTO, ONTARIO

SEPTEMBER 2022

ABSTRACT

The enhancement of medical tattoo electrodes over the past few decades have progressively allowed them to serve as a superior alternative to conventional Ag/AgCl electrodes. Given their structure, these electrodes can seamlessly conform to the skin and last over longer periods of time. In addition, additive manufacturing methods can enable efficient and flexible fabrication of the tattoo electrodes. The objective of this project is to optimize printing methods to fabricate medical tattoo electrodes, as well as analyze and compare their performance both in vitro and in vivo to the gold standard electrodes. In the first part of the project, inkjet and extrusion printing methods were optimized to print various electrode patterns on a tattoo paper substrate. Additional steps were taken during and after inkjet printing to further improve the functionality of the electrodes. The novelty of this part was presented through the extensive experimentation of printing viscous and non-viscous metal-based inks on tattoo paper and the simple contact platform developed to allow for external connections to rigid components. The second part of the project involved the initial testing and analysis of the electrical and mechanical performance of the electrodes outside the human body. This was specifically studied with impedance tests to acquire information at the skin-electrode interface, as well as bending tests to analyze the impact of mechanical deformation toward the electrical performance. In the final part of the project, the electrodes were tested on human subjects to acquire ECG and EMG signals, which were analysed in terms of signal quality.

ACKNOWLEDGEMENTS

I would like to take the opportunity to extend my gratitude to those who supported me during my time in the MASc program. First, I would like to sincerely thank my supervisor Dr. Gerd Grau for his continuous support during my time as a Master's student. I am appreciative of his ongoing assistance, patience, and encouragement, especially in the early stages of my research when I was unable to work physically in our lab. Also, I would like to thank Dr. Ebrahim Ghafar-Zadeh who kindly agreed to join my supervisory committee and was keen to learn about and support my research. I would like to thank Dr. Will Gage for generously agreeing to participate in my oral examination.

I want to thank Giancarlo Ayala-Charca for his continued assistance during the in vitro and in vivo testing stages of my project. I would also like to thank Magdalena Jaklewicz at the Advanced Light and Electron Microscopy Facility for providing exceptional assistance when examining my samples under SEM. In addition, I would like to formally acknowledge the Natural Sciences and Engineering Research Council of Canada (NSERC) for their support.

I want to extend my gratitude to my fellow labmates, especially Milad. He was very supportive and provided me with extensive assistance at a time when I was learning to navigate my way as a researcher during the COVID-19 pandemic. I would also like to thank Mohamad K. and Mohammed N. (Syrian and Iranian Mohamed respectively) for making my time in the lab more enjoyable. Lastly, I am grateful to have worked alongside and become friends with Paria, who is the crazy lab lady every lab should have.

Lastly, I would like to thank my friends and family for their never-ending support and encouragement during tough times.

TABLE OF CONTENTS

LIST OF TABLES

LIST OF FIGURES

CHAPTER 1. INTRODUCTION

1.1. Medical Electrodes

Physiological systems in the human body can have electric activity associated with bioelectric phenomena related to the distribution of ions or charged molecules in biological structures. These phenomena can be potentially extracted and used for diagnostic or functional purposes, particularly with signals that are high-level and time-varying [1]. Common signals such as electrocardiograms (ECG), electromyograms (EMG), and electroencephalograms (EEG) present vital information pertinent to the heart, muscle, and brain, respectively. Other signals that are of interest include EOG (eye dipole field), EGG (stomach), and GSR (galvanic skin response) [1]. By acquiring these signals, ailments associated with these biological systems can be diagnosed, and the signals can serve as an input into actuator based medical devices.

To effectively acquire biophysical data, medical electrodes are implemented to convert ionic charge carriers into electronic currents, which can be interfaced with a data acquisition system to ultimately display and analyze the data. Redox (reduction-oxidation) reactions between electrons in electrodes and ions in the body need to occur for a charge to be transferred between the two surfaces. Between a metal in contact with a solution of its ions, a half cell potential is established in which the electrolytic solution surrounding the metal has a different charge [1]. This potential exists when there is no electric current flowing between both interfaces, and the potential can subsequently be changed when there is current present. This is caused by a process called polarization, where there is a change in charge distribution within the electrolytic solution. Ideally, there should be no change in charge distribution at the electrode-electrolyte interface and the electrodes should be able to allow current to easily pass at this interface. Electrodes of this nature are non-polarizable and perform well when under conditions involving applied motion and low frequencies [1].

1.1.1. Electrical Characterization

Under idealized conditions, the skin-electrode interface can be represented with a simple electric circuit, seen in Figure 1-1. This circuit is based on the Cole bioimpedance model [35] In the circuit the resistor Rd and capacitor Cd in parallel represent the impedance associated with the electrode-electrolyte interface and polarization at this interface. The series resistance Rs is associated with interfacial effects and the resistance of the electrode materials themselves. Ehc represents the half-cell potential and is shown as a battery in the model [1].

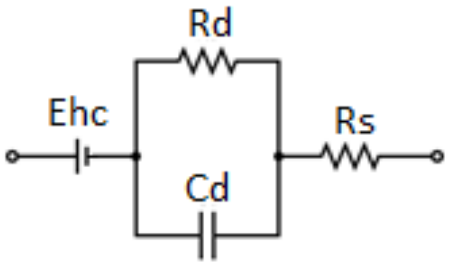

Figure 1-1. Biopotential Electrode Circuit Model (under idealized conditions)

Impedance within the aforementioned model is a vital factor to consider and should ideally be minimized to improve signal quality. With a high impedance, there is a strong barrier between the skin and electrode which prevents the transfer of biopotentials [36]. Increasing electrode surface area, surface roughness and radius of curvature can reduce the impedance, while an increase in polarization (at lower frequencies) and surface contamination can increase it [1]. A sample trend for biopotential electrode impedance over a range of frequencies can be seen in Figure 1-2, although it is important to note that this behavior can vary from one type of electrode to another.

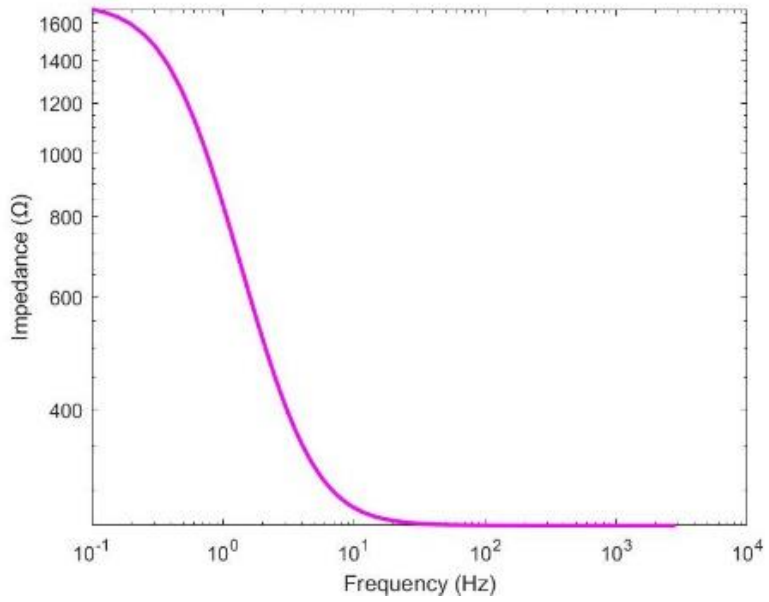

Figure 1-2. An example of biopotential electrode impedance as a function of frequency (from 0.1 to 100k Hz).

1.1.2. Commercial Biomedical Electrode Types

There are several types of electrodes used for the purpose of performing biopotential recordings, with their structures designed to work in various medical contexts. The types of electrodes discussed are non-invasive, with the intention of being placed on the surface of the human body as opposed to invasive/needle electrodes injected within the body.

Metal plate electrodes and disposable hydrogel electrodes are commonly implemented electrodes composed of a metallic layer contacting the skin with an electrolytic gel layer in between, as shown in Figure 1-3a. For these electrodes there is a slight difference in the shape, conductive materials and overall configuration. Due to the flat structure of these electrodes, they are commonly used on areas of the body that are flat as well, such as the chest, wrist, ankle, etc. Metal disk electrodes are a form of metal plate electrode used for EEG recordings given the advantage of their conical shape [1]. Since metal based electrodes are inherently rigid and rely on an electrolytic

component that eventually dries out and/or has to be replaced, they are generally used for short term monitoring.

In contrast, long term monitoring of biopotential signals can be accomplished with dry, thinner, and more flexible electrodes. A step toward this has been with the implementation of recessed electrodes consisting of an electrode interfacing with an electrolytic gel, secured to the skin with a surrounding flexible adhesive (see Figure 1-3b) [1]. Thin film electrodes are a more comfortable and conformable form of electrode that have been used to monitor vital signs in neonates [1]. These electrodes last longer on the skin, preventing the need to replace electrodes and potentially causing irritation to the skin (see Figure 1-3c). Carbon elastomer dry electrodes deviate from the previously mentioned types of electrodes to serve a more niche purpose such as cardiorespiratory monitoring for infants [1]. Dry electrodes improve in performance over time due to the presence of sweat beneath the electrodes, essentially serving as a natural electrolytic solution [1].

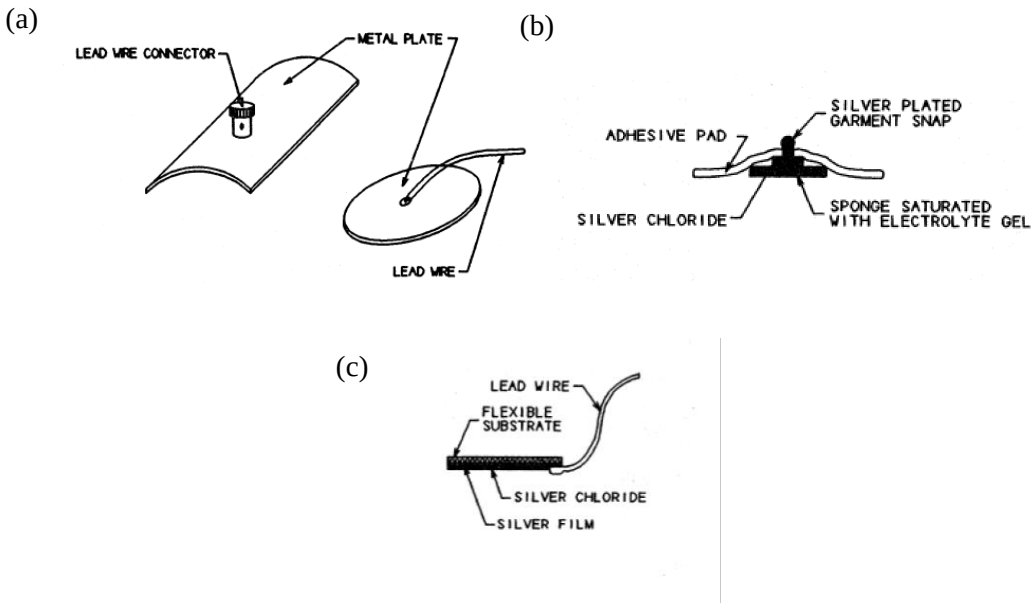

Figure 1-3. Types of biopotential electrodes including (a) metal-plate, (b) recessed, and (c) thin film electrodes [1]

Medical tattoo electrodes have gained more popularity as an alternative to traditional medical electrodes particularly for long term healthcare monitoring, as they are they are lightweight, conform to the skin, and can be made with a variety of conductive materials. These forms of electrodes seamlessly rest on the skin, conforming to contours on the body and even allow hair to grow through. Tattoos enable skin breathability and have a comparably higher permeability coefficient for water vapour compared to thicker substrates used for other electrodes [10]. In addition, organic [8] and inorganic [7] materials have been previously used to demonstrate functional medical tattoos, although there has not been extensive use of the latter set of materials. Common materials and fabrication methods used to form these medical tattoos will be discussed in the following sections.

1.1.3. Conventional Electrode Fabrication

Conventional medical electrodes typically found in clinical settings are fabricated layer by layer, with a majority of the design process dedicated to accommodating other elements of the design (i.e. wires, adhesive backing) with the central conductive material [3]. Generally, the conductive material is designed to interface with an electrolytic solution and an external contact. For example, Ag/AgCl electrodes commonly found in North America have an Ag based male-connector snap that comes in contact with an electrolytic solution from the bottom and can be connected to a wire with a female-connector at the top (Figure 1-3b). An adhesive pad, which is placed on top of the electrode with a cut-out for the male-connector snap, is used to secure the electrode onto the body. These electrodes are fabricated via a layer-by-layer process in large-scale industrial settings, where the silver snap is placed on the electrolytic component and the adhesive pad is then placed on top. The snap closures, which are also found in regular clothing, are made using stamping and/or die-casting processes [2]. Even the thin film electrodes shown (Figure 1-3c) are made layer by layer, by securing a conductive film onto a flexible substrate such as polyimide [1].

1.2. Unconventional Medical Electrodes

Over the past two decades, new forms of medical electrodes have been developed to perform as well as or better than conventional electrodes, while also conforming more seamlessly to the human body. These electrodes can come in the form of flexible sensors, textiles, and tattoos, each made with a variety of materials and fabrication methods. To obtain biophysical signals, these electrodes are especially beneficial to use as they can withstand extensive mechanical deformation (i.e., strain), which is often present when acquiring these types of signals. The following sections will discuss different unconventional electrodes specifically used for electrophysiological signal acquisition.

1.2.1. Flexible and Textile Electrodes

Numerous flexible and textile medical electrodes have been developed over recent years in academic and R&D spaces. These forms of medical electrodes allow for more robust acquisition of biophysical data, can potentially be reused, and can be integrated with day-to-day items such as clothing and wearable sensors.

An earlier example of textile-based electrodes is by Yoo et al. [25], who developed a "planar-fashionable circuit board (P-FCB)-based shirt". The shirt incorporated dry electrodes that were screen printed, which directly formed a contact to an ECG monitoring chip. Stencil printing and dipping was used by Jin et al. [26] to develop an EMG monitoring garment with multiple channel electrodes acquiring signals to examine muscular activity on different points along a subjects' arms. The previously mentioned textile electrodes were made from silver flake inks, which have been proven to work well on textile surfaces. Screen printing was also used by Xu et al. [6], where a graphene-based ink was screen printed on a modified textile. The resulting pattern was used as an electrode to acquire ECG signals, and the overall textile exhibited suitable characteristics, such as high flexibility and resistance to degradation after multiple washes.

Sputtering of copper [33] and gold [25] materials has also been implemented to fabricate conductive patterns on textiles.

Flexible electrodes can be made on a variety of substrates and can be made with a wide range of fabrication methods. Scalisi et al. [27] developed flexible electrodes used to acquire surface electromyography (sEMG) signals. These electrodes were fabricated by inkjet printing a commercial silver ink on a polyimide (PI) substrate and were designed to form an sEMG electrode array. Flexible ECG electrodes were fabricated by Chlaihawi, et al. by screen printing silver flake ink on a polyethylene terephthalate (PET) substrate [24]. A medical electrode with a pyramidal array was developed by Wang et. al [28] to reduce contact impedance. The electrode was formed using an etched silicon mold used to shape polydimethylsiloxane (PDMS) as it was spin coated. Then parylene was added on the PDMS via chemical vapor deposition (CVD) and a layer of gold was sputtered on top.

1.2.2. Medical Tattoo Electrodes

Compared to flexible skin-mountable sensors, tattoos are generally thinner, conform more seamlessly to the skin, and last over longer periods of time. Temporary tattoos can be held in place solely with Van Der Waals forces [60]. Tattoo paper, the material that is used to anchor the desired pattern, is low-cost, mass produced and accessible, and has a low environmental impact [59]. This substrate is generally in the form of a water slide decal, which has a sacrificial layer atop of a water-resistant paper backing [10]. The desired pattern is added on the sacrificial layer, and an adhesive layer can be added on top of the printed pattern to help hold the pattern in place on the skin [10]. These tattoos have been used in a wide range of biomedical applications, from electrophysiological and biochemical sensing to drug delivery [61]. Tattoo electrodes demonstrated specifically for the acquisition of biophysical signals will be further discussed.

Numerous studies have implemented inkjet printed tattoos with various, predominantly organic, conductive materials. Poly(3,4-ethylenedioxythiophene) polystyrene sulfonate or

PEDOT:PSS has been a material of interest for the application in discussion due to its electrochemical stability and due to the fact that it can be dispersed with different means to form inks suitable for a range of fabrication methods [23]. Bihar et al inkjet printed PEDOT:PSS onto tattoo paper and a corresponding textile contact to integrate the tattoo with a signal acquisition system used to collect EMG signals [23]. PEDOT;PSS based electrodes were also formed by Taccola et al [29], and were integrated with a robust docking mechanism to enable external connections for the acquisition of ECG and EMG signals. Another example of PEDOT:PSS based inkjet printed tattoo electrodes was demonstrated by Ferrari et al.[8], which were implemented for the acquisition of EEG signals. Two consecutive PEDOT:PSS layers were printed on tattoo paper to lower the sheet resistance of the electrodes. The tattoos can be seen alongside a conventional electrode in Figure 1-4.

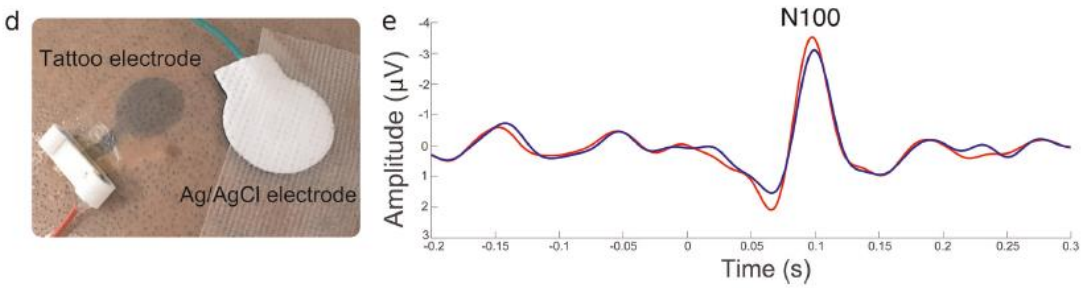

Figure 1-4. Temporary tattoo electrode (TTE) and Ag/AgCl electrodes on the head of the participant (left). Auditory evoked potential recorded with both TTEs (red) and Ag/AgCl electrodes (blue), with N100- an auditory evoked potential component (right). Reproduced with permission [8]. Copyright © 2020, Springer Nature Publishing Group

Another material, graphene, was used by Ameri et al. [9] to form an electronic tattoo via a "wet-transfer, dry-patterning" method (see Figure 1-5). The resulting tattoos were used to examine multiple vitals, including ECG, EMG, and EEG signals, as well as skin temperature, and skin hydration. A similar "cut and paste" method was employed by Ha et al. [64] to apply a mechanically cut polyvinylidene fluoride (PVDF) film onto a medical tape substrate. The resulting tattoo-like

sensor was used to perform seismocardiography (SCG) which is the measure of chest vibrations associated with heart beats [64].

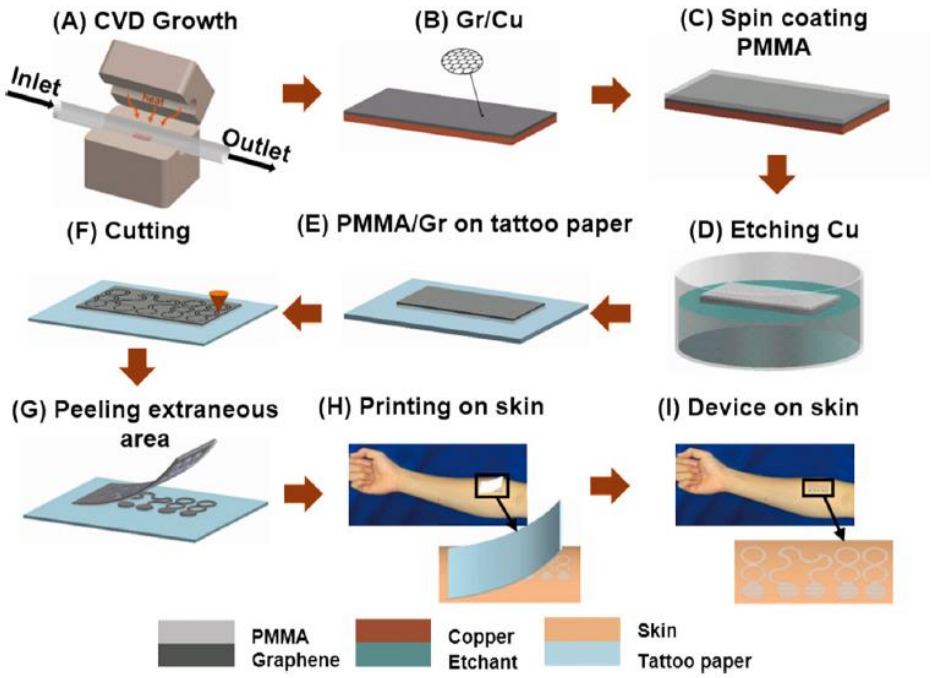

Figure 1-5. Fabrication process of Graphene Electronic Tattoo or GET. (A-G) "Wet-transfer, dry patterning" fabrication method (G-I) Placement of GET on skin. Reproduced with permission [9].

A wireless, battery-free acquisition circuit was developed with selectively applied silver Gallium-Indium (Ag-In-Ga) traces on a non-conductive inkjet printed pattern [34]. The resulting circuit was used to acquire ECG signals with energy supplied with a "wireless power transfer (WPT)" system.

Screen printing has also been used to print electrodes on tattoo paper. A screen printed pressure sensor for pulse detection was demonstrated by A. Peplowski et al [67]. The sensor was fabricated with carbon nanotube (CNT) and graphene nanoplatelet (GNP) based pastes. Skintillates is a screen-printed electrode developed by a group of students from UC Berkley, which is in the form of a tattoo with printed silver traces atop of an artistic design [7]. Carbon-based ink was screen

printed on tattoo paper to form electrodes used to acquire EMG signals, as demonstrated by Barekat et al [30]. In the aforementioned example by Taccola et al [29], screen printed silver tracks were added alongside the PEDOT:PSS tattoos to connect to a magnetic docking mechanism.

1.3. Printing Methods

A disadvantage of the manufacturing procedure for conventional electrodes is that the electrodes cannot be easily customized, and the range of materials used is limited. To this end, printing based fabrication can enable flexibility in the design and material aspects of the electrodes while still ensuring the fabrication is cost and time efficient. In the area of printed electronics, processes including screen and inkjet printing have been implemented to address the limitations set by conventional electrode fabrication methods. These processes have largely been used to develop flexible electrodes in the form tattoos, which further solve the conformability issues posed by conventional electrodes.

There are several requirements for printing with regards to the materials and settings used. The materials, which primarily include ink and a substrate, must possess specific characteristics to acquire a desired printed result, and at times are chosen in accordance to each other. These materials are selected to suit the intended application, while accommodating the restrictions posed by the printing method used. The settings/parameters chosen during the printing process must allow suitable dispensing of the ink on the substrate.

When printing tattoo-based electrodes specifically, there are several interfacial considerations such as the morphology of the substrate (tattoo paper) and the interaction of the selected ink with said substrate. Like the treatment of textiles for the addition of a screen-printed functional pattern, tattoo paper can also be modified [10]. A review on the use of tattoo paper for conformable electronics in medical applications examined two available tattoo paper substrates (see Figure 1-6). Given that tattoo paper is porous, inks at a lower viscosity are susceptible to absorbing or spreading on the surface. For this reason, viscous (i.e. screen-printable) inks have an advantage over inks used

within inkjet printing. If optimized however, inkjet printing can form patterns with higher resolution and lower thickness.

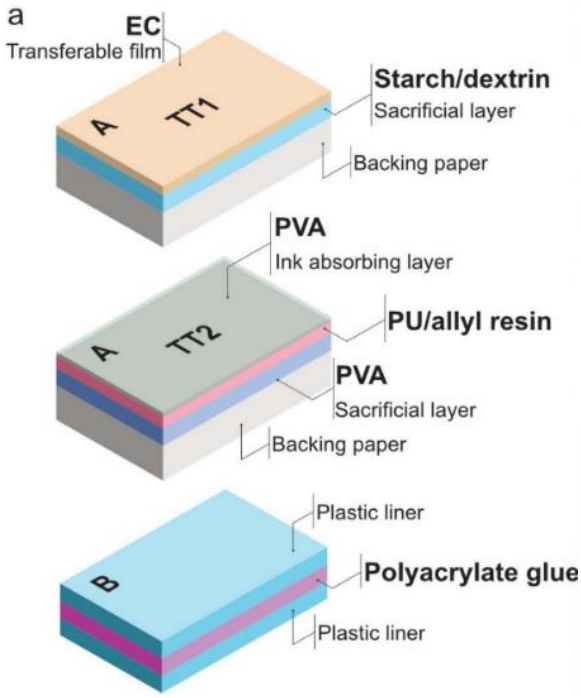

Figure 1-6. Types of temporary tattoo (TT) paper (a): water slide decal sheet A—schematics of layers in types TT1 and TT2; adhesive sheet B to be laminated on top of A. Reproduced with permission [10]. Copyright © 2018, Institute of Physics Publishing Ltd.

The primary functional component during the printing process is the selected ink, which mainly consists of a solute, solvent, and additives (as needed). The solute (includes polymer-based, carbon-based, organic and inorganic materials) is suspended in the solvent, with the additives serving an additional function. There are many options for potential substrates, such as plastic (polymer-based), glass, paper, etc, which can be chosen based on the application in mind. The surface roughness and surface energy of the substrate are important properties to consider when making a selection, as they can potentially improve or worsen the desired pattern once the ink comes in contact with them. After the printing process, additional steps should be taken to remove

the solvent within the printed ink (a process known as drying) and enable complete functionality of the solute.

While the application of printing methods toward the development of medical tattoo electrodes has been explored, minimal work has been done to optimize the printing process and further exploit the benefits of printing, i.e. compare different electrode designs. In addition, extrusion printing has not yet been implemented in the development of medical tattoos.

1.3.1. Inkjet Printing

Inkjet printing involves the deposition of a functional (i.e. conductive, insulating) material on a substrate in a droplet form that approximately corresponds to the size of the nozzle diameter used [4]. This printing method uses a low viscosity ink (1-20 mPas), and creates thin (0.3-20 μm) and high resolution (>50 μm) patterns [5]. It is a popular printing method both within and outside (home, office, etc.) and in the field of printed electronics. Drop on demand (DOD) printing involves the deposition of separate drops, as opposed to depositing drops continuously. In this form of inkjet printing, a piezoelectric actuator is controlled by a unipolar/bipolar waveform of potential with time. The DOD printing process can be seen in Figure 1-7a.

(a)

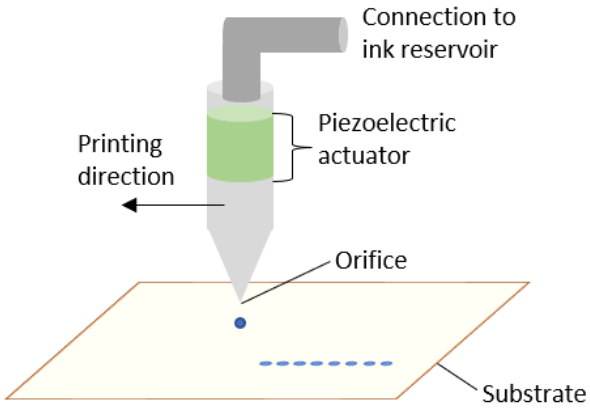

(b)

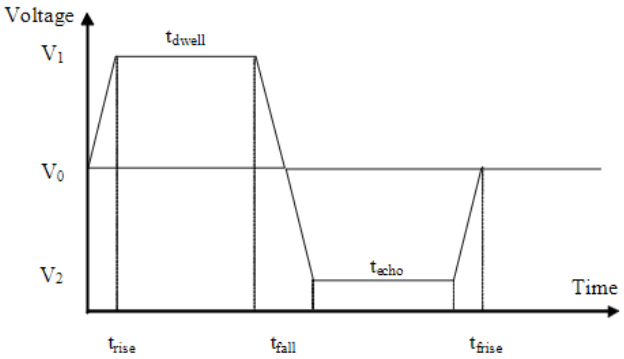

Figure 1-7. (a) DOD printing process, (b) Bipolar actuating waveform [22]

In contrast to a simple unipolar waveform, a bipolar waveform consists of a negative pulse or "echo" [22]. Jetting parameters for the printer should be set accordingly to form a waveform and promote proper jetting of the ink. For a bipolar waveform, these parameters include Rise/Dwell/Fall Time and Dwell/Echo/Idle Voltage, which are chosen accordingly to prevent the occurrence of jetting issues such as the satellite effect [22]. The spacing between the drops and speed of the deposition of the drops can also be optimised to form a desired pattern. It is vital that these parameters are optimized to prevent bulging or separation between drops, of which both occurrences can impact the performance of the resulting design. Characteristics such as viscosity and surface tension of the given ink are especially critical to consider during inkjet printing. Inks

with low viscosities are required to avoid clogging the inkjet nozzle [31], but the inks should also have a high enough surface tension to prevent leakage [32].

1.3.2. Screen/Extrusion Printing

During the screen-printing process, a functional ink is penetrated through a stencil within a mesh and deposited onto a substrate, creating the desired pattern [4]. Compared to inkjet printing, this form of fabrication requires a more viscous ink (1-100 Pas), and results in patterns that are fairly thick (3-25 μm) and low in resolution (>100 μm) [5]. This printing method is commonly used to print patterns onto textiles in the fashion industry, as well as signs, displays, labels, and so on.

Extrusion printing is a "digital" alternative to screen printing, which functions similarly to some forms of 3D printing, but is primarily used to print 2D patterns in the field of printed electronics. This allows for more flexibility with the patterns printed as extrusion printing does not require a printing master. This can be particularly beneficial when developing medical devices/sensors as the resulting design can be tailored to suit different users. Akin to screen printing, extrusion printing can be used to print on porous and/or rough substrates more effectively than methods such as inkjet printing.

During extrusion printing, a piston component within the printer head is displaced to reach a pressure high enough to extrude a given ink from the end of the nozzle. Parameters such as dispensing height and relief pressure can be experimentally obtained to acquire the desired thickness of an ink on a given substrate. The extrusion printing process can be seen in Figure 1-8.

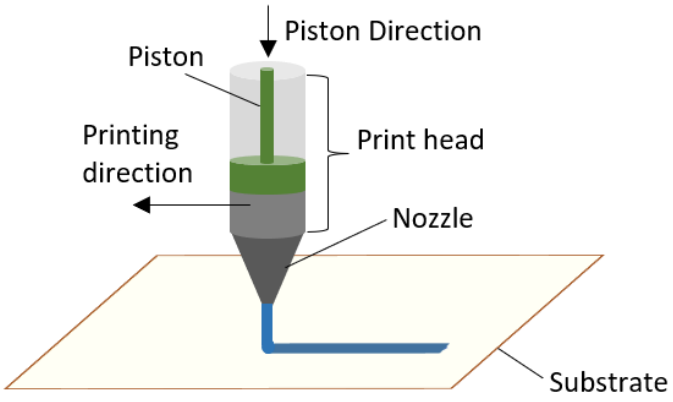

Figure 1-8. Extrusion printing process

1.4. Printing Materials

To develop applications used in a biomedical context using printing methods, additional considerations need to be made pertaining to the functional materials used. Biocompatibility is an important factor to consider, as the resulting component developed is interfacing directly with the human body to serve a particular purpose (i.e. acquire biophysiological signals). There should be no irritation or toxicity induced by the materials used, more notably for the ink as that serves as the active component within the overall fabricated device. In addition, the materials should accommodate the applied stresses due to human motion and thus be mechanically durable. The main electrode materials used to print medical tattoo electrodes, including organic (graphene, PEDOT:PSS), and metal (gold and silver) based inks, will be discussed.

Graphene, which is a monolayer of carbon atoms bound in a hexagonal lattice [15], has been a preferred material for the development of medical tattoo electrodes using printing methods. This material possesses desirable electrical and mechanical properties, such as high charge carrier mobility, superlative thermal and chemical stability and intrinsic flexibility [16]. Graphene based inks offer a low-cost alternative with excellent environmental stability and desirable conductivity

[16]. When produced with a polymer stabilizer, stable and high-concentration graphene dispersions can be formed in a range of solvents including ethanol, terpineol, and cyclohexanone [16].

Another commonly used material for the development of printed tattoo electrodes is PEDOT:PSS, which is a transparent conductive polymer consisting of a mixture of poly(3,4-ethylenedioxythiophene) and polystyrene sulfonate [17]. The mechanical and electrical properties of PEDOT:PSS can be tailored by modifying its molecular structure, although both cannot be optimized simultaneously [18]. Solvents such as dimethyl sulfoxide (DMSO) [18] and ethylene glycol [19] have been used to adjust the viscosity and its electrical properties accordingly to allow for use in a range of printing methods.

Compared to polymer- and carbon-based inks, metallic (gold, silver, etc.) inks are more robust in terms of electrical and mechanical performance making them suitable for the development of the application in discussion. Printable forms of these materials include silver/gold nanoparticles, nanowires, flakes, etc., and these materials can be synthesized with chemical and physical methods [20]. In nanomaterial form, gold is known for its high conductivity and biocompatibility, surface plasmon resonance and special optical and electronic properties [21]. Although less susceptible to oxidation compared to other metals, gold is more expensive. Silver is a suitable alternative to gold as it possesses similar qualities but is comparatively more inexpensive. It is preferred due to its high electrical and thermal conductivity, high chemical stability, low melting point, and relatively low cost compared to other materials [11].

To allow silver to be printed with an inkjet printer in the form of an ink, work toward the synthesis of nanomaterials and surface-modification techniques has enabled silver to be dispersed in organic solvents or water with surfactants added as needed. For printing methods requiring inks at a higher viscosity, such as extrusion printing, flake-based inks are suitable as the flakes are in the micron scale. Conversely, nanoparticle-based inks tend to have a lower viscosity and are thus appropriate for methods such as inkjet printing. To be used for printing purposes, these silver nanoparticle and flake solutes are combined with a solvent (e.g. methanol, ethanol [21], PGME

[14]) and functional additives such as binders. Due to the variation in ink composition and active material structure, the annealing process for nanoparticle and flake ink can differ. For flake-based inks, most additives must be removed to allow the flakes to interact and conduct current, but components such as the binder should stay to allow the ink to adhere to the substrate [40]. On the other hand, annealing of nanoparticle inks typically involves the removal of any additives to form a percolation network by necking/merging of particles [41]. To avoid the use of high temperatures during the annealing process for substrates such as paper, intense pulsed light (IPL) sintering can be used [42]. This sintering method involves the application of high intensity light flashes over a given sample within a short period of time (micro- to milli-seconds) [43]. Given that the light is absorbed by only the metal component of the sample, the substrate beneath is not impacted.

The use of silver-based inks can serve as a more electrically/mechanically robust and accessible alternative to the predominantly organic inks used for the majority of medical tattoos formed thus far. Experimenting with varying silver-based ink types can provide further insight toward tattoo electrode performance based on varying tattoo thickness and composition.

1.5. Thesis Organization

In this thesis, a study of silver-based medical tattoo electrodes fabricated with printing-based methods is presented. Post-fabrication, the electrodes are demonstrated in the acquisition of biophysical signals.

In chapter 2, the fabrication process of the medical tattoo electrodes using inkjet and extrusion printing methods and subsequent characterization is discussed. The respective methods are optimized to develop silver-based patterns on tattoo paper with suitable morphological characteristics. Further optimization of sintering, i.e. IPL, processes for inkjet printed tattoos is also discussed.

In chapter 3, in vitro testing of the tattoo electrodes was completed, including impedance and bending tests. A phantom model was implemented to examine the electrical behaviour of the

electrode at a range of frequencies. In addition, bending strain was applied to the electrodes at varying radii to examine the impact of mechanical deformation toward electrical performance.

In chapter 4, human tests of the tattoo electrodes were performed to examine the efficacy of the tattoo electrodes toward their intended application. ECG signals using tattoo electrodes of various shapes were acquired from human participants and compared to conventional medical snap electrodes.

In chapter 5, the primary findings of this thesis are outlined, and suggestions for relevant future work are proposed.

CHAPTER 2. PRINTED SILVER INKS ON TATTOO PAPER

2.1. Introduction

There is a large potential for the fabrication of medical tattoo electrodes using printing methods, and with the use of more robust materials. The majority of these medical components developed in academia have relied on traditional processes such as photolithography, chemical vapor deposition (CVD), and sputtering, and typically involve more than one of these processes. Compared to printing methods, these forms of fabrication are more expensive and require the use of complex equipment. Printing-based techniques can provide numerous benefits for these medical components, such as flexibility in the materials used and patterns printed, personalization of the electrode design, and potentially low cost. This may be not as simple to do with a method such as sputtering, which would require the use of a mask. In addition, more electrically and mechanically robust materials can be implemented as long as they can be printed. The optimization of inkjet printing patterns on tattoo paper has not been fully explored in the literature, and extrusion printing has also not been used to develop medical tattoo electrodes.

Previously developed medical electrode tattoos can serve as a benchmark when forming the same sensors with new fabrication methods and materials. Medical tattoo electrodes reported previously have a sheet resistance in the range of 41 mΩ/□ [45] to 1994.33 ± 264 Ω/□ [9] using different conductive materials (silver and graphene respectively). To this end, inkjet and extrusion printed tattoo medical electrodes were developed to examine bioelectric phenomena within the body. Upon comparing several types of inks, silver-based inks were selected due to their suitable electrical and mechanical properties, biocompatibility, and accessibility. A version of this chapter has been published in Y. El-Hajj, M. Ghalamboran, and G. Grau, “Inkjet and Extrusion Printed Silver Biomedical Tattoo Electrodes,” in 2022 IEEE International Conference on Flexible and Printable Sensors and Systems (FLEPS), Jul. 2022, pp. 1–4. Doi: 10.1109/FLEPS53764.2022.9781535.

2.2. Printing Electrodes on Tattoo Paper

4 mm by 4 mm squares were printed on commercial tattoo paper (Silhouette Temporary Tattoo Paper, USA) using inkjet and extrusion printing. Other shapes, including circles with a diameter of 4 mm, and 4 mm by 4 mm spiral matrices were also printed.

A field emission scanning electron microscope (FE-SEM) (Thermofisher Quanta 3D) was used to further understand the interaction between the AgNP ink and tattoo paper substrate. Drying the samples in a vacuum allowed the sample to be degassed and promote a stronger signal when taking the images. Figure 2-1 shows the difference between a hot plate and vacuum oven dried sample.

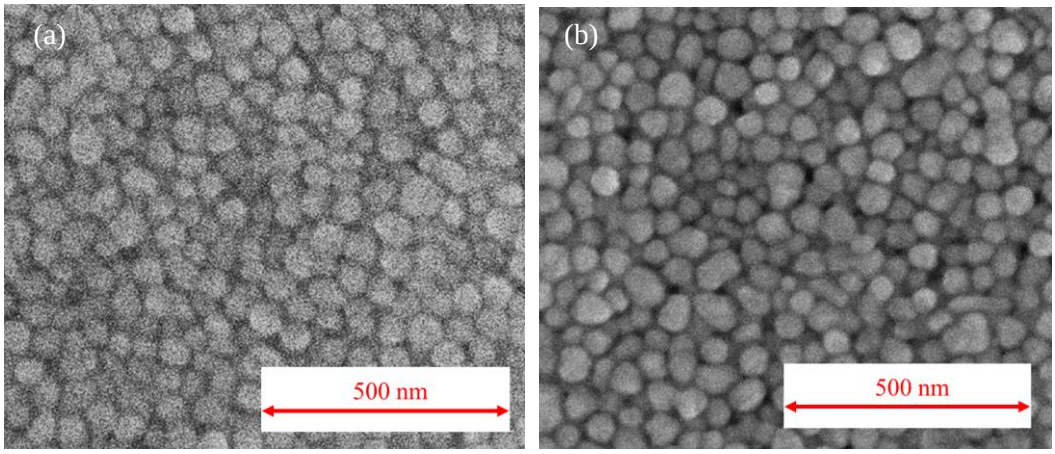

Figure 2-1. SEM images of 3 layer electrodes dried (a) on a hot plate, and (b) in a vacuum oven at 100ºC for 30 minutes

The surface morphology of the tattoo paper was examined to further understand the substrate used and tune the printing process accordingly. As seen in Figure 2-2, the surface of the tattoo paper possesses a random distribution of shallow pores, with one pore size recorded to have a diameter of approximately 40 µm.

(a)

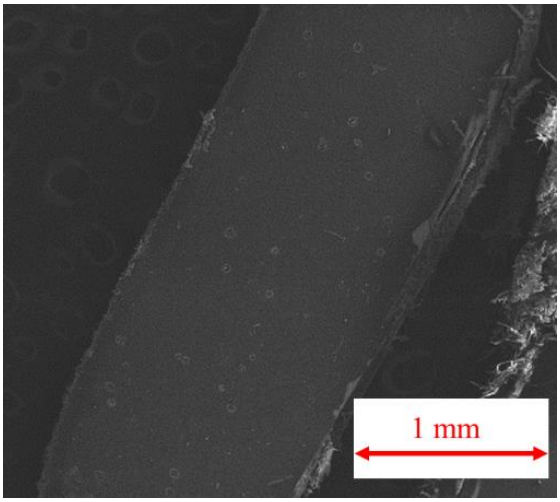

(b)

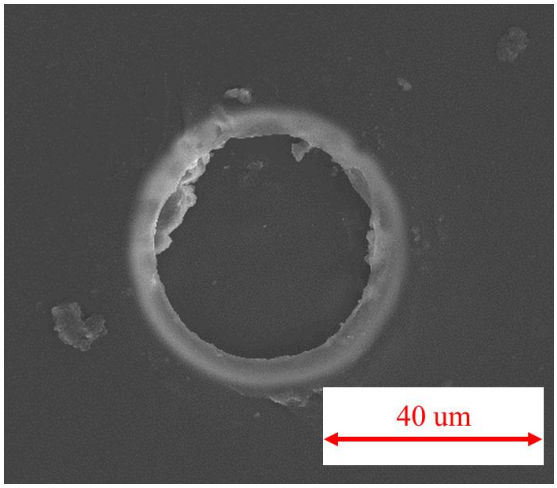

Figure 2-2. SEM images of (a) top view of tattoo paper, and (b) pore in tattoo paper

Analysis of the surface morphology of the tattoo paper was completed with optical profilometry (Bruker Contour GT-K 3D Optical Profiler). Initially, stylus profilometry was used to examine the surface of the tattoo paper. However, due to the soft surface of the substrate, the force applied was too high, resulting in inaccurate scans. Optical profilometry allows for non-invasive analysis of the sample surface and was therefore chosen. The surface morphology of a plain, clean tattoo paper surface can be seen in Figure 2-3.

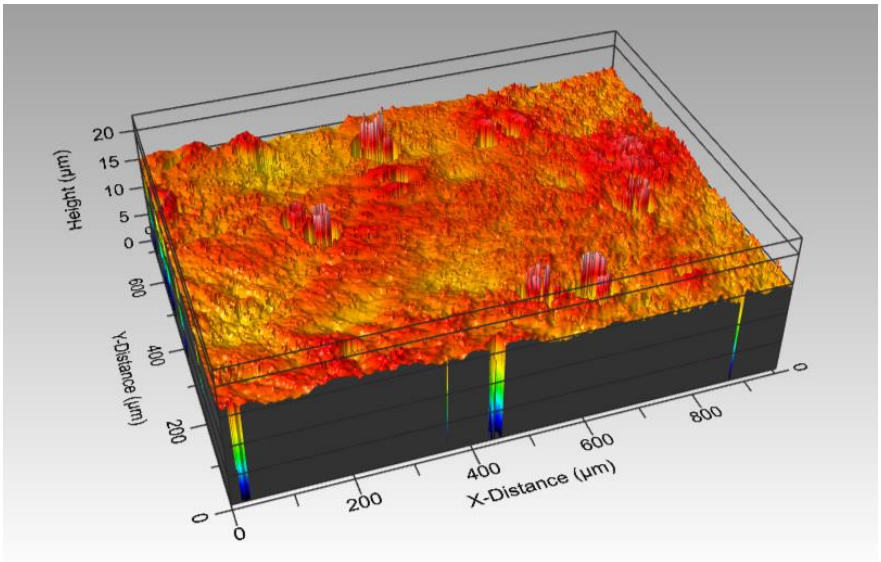

Figure 2-3. Plain tattoo paper surface

For inkjet printing, silver nanoparticle (AgNP) ink (ANP DGP 40LT- 15 C, Advanced Nano Products, Co., Sejong, Korea) was used. Prior to printing, the tattoo paper was attached on a glass substrate (Fisherbrand Precleaned Microscope Slide) with tape to create an even printing surface and purged with air to remove any dust. To deposit the ink on the tattoo substrate, a custom-built inkjet printer with a 60 µm diameter nozzle (MJ-ATP-01-60-8MX, Microfab Technologies, Inc. Plano, TX) was used. The jetting parameters were taken from previous experimentation[41], and a drop spacing of 80 µm was used to obtain the desired pattern. This drop spacing was found experimentally based on the interaction between the ink and substrate. The square pattern printed was printed in a raster format.

Two by two mm squares were inkjet printed to conduct experiments related to the study of sheet resistance. Initially, only one layer of AgNP ink was printed on the tattoo substrate. Upon further inspection of the printed pattern on the substrate with a light microscope, there were consistently areas in the square pattern that were missing ink and there were numerous pores visible. This was to be expected and is a common issue when printing low viscosity inks on porous substrates, as the ink would have been partially absorbed into the paper [46]. Therefore, to ensure

sufficient pattern integrity, one to five layers of the AgNP ink were printed on the tattoo paper substrate (see Figure 2-4). With an increase in layers, the number of pores within the pattern was reduced, although there were still some pores visible even with five printed layers.

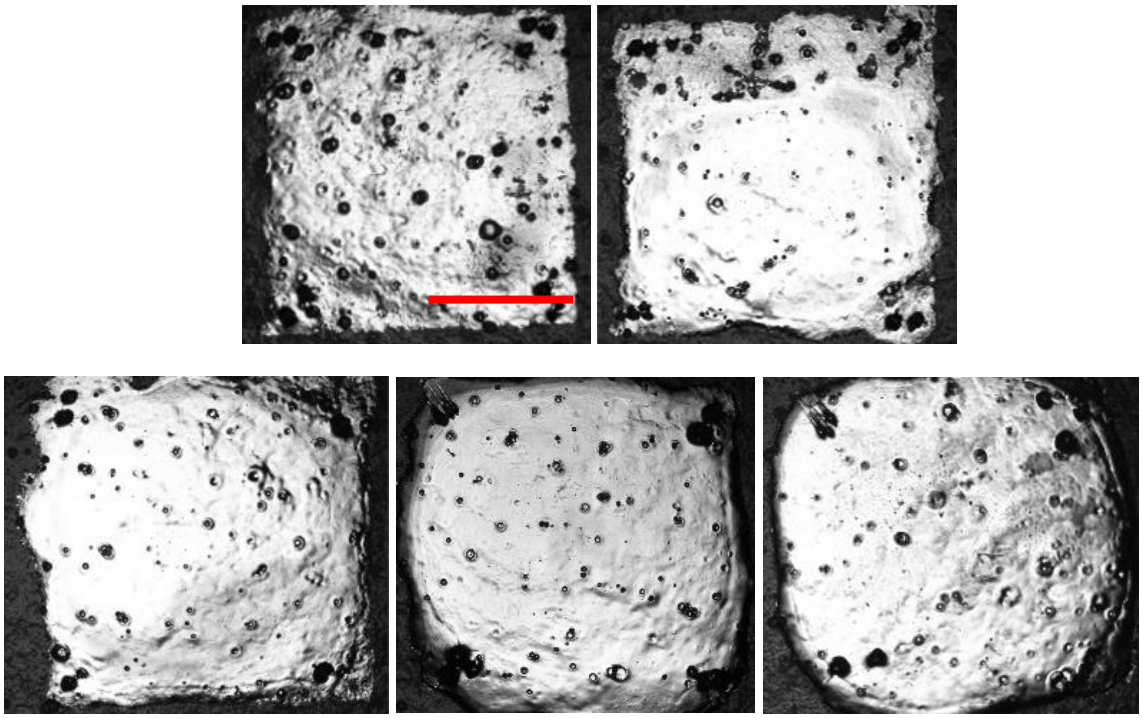

Figure 2-4. Light microscope images of post-annealed AgNP ink squares with 1 to 5 layers (top left to bottom right) on tattoo paper. The scale bar indicates 1 mm.

Sheet resistance measurements were conducted based on the Van der Pauw method [47] using a Semiconductor Parameter Analyzer (Keithley 4200A-SCS, Tektronix, Beaverton, OR). The data was analyzed in MATLAB 2021a, to calculate the sheet resistance of the squares.

The sheet resistance for the dried inkjet printed electrodes was measured and compared for one to five layer square patterns (see Figure 2-5). The expected trend between these two parameters would be linear, as the sheet resistance would theoretically decrease with each added layer. However, this did not correlate with the observed trend. From one to three layers, the sheet resistance was relatively high and possessed a large variability in the values acquired. After

printing four layers, the sheet resistance decreased to 64.8 ± 13.3 mΩ/sq and plateaued after printing more layers. The values obtained also reduced in variability, indicating that the electrical behaviour of the patterns is more consistent. Although the resistance was reduced significantly, the pattern definition was also reduced as shown in Figure 2-5.

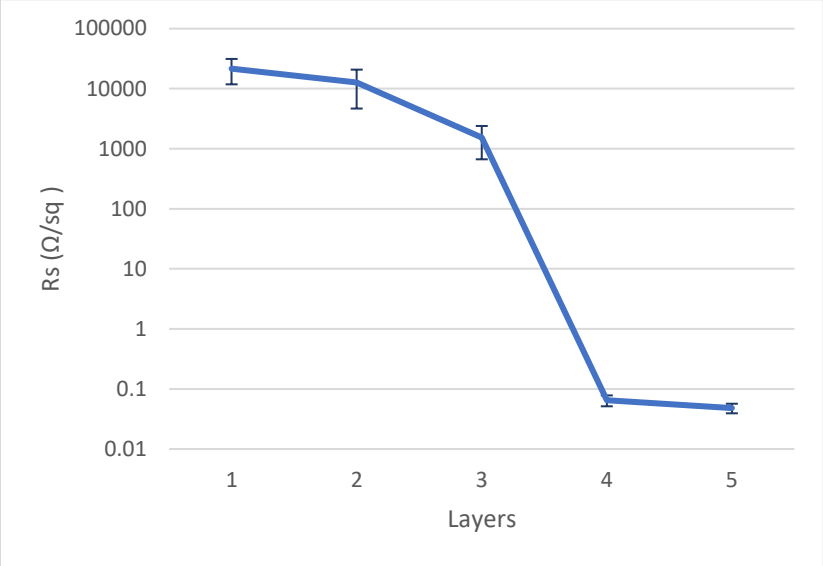

Figure 2-5. Sheet resistance versus number of printed AgNP ink layers. Note that the electrodes were only dried for 30 minutes at 100ºC

Extrusion printing was performed with an extrusion printer using a 150 μm diameter nozzle (Voltera NOVA, Kitchener, Canada). The printing materials, including the tattoo paper and silver flake ink (Creative Materials 120-07, Ayer, USA), were utilized during the calibration of the printer, which calculates the dispensing height for the nozzle relative to the substrate, and the pressure required to move the ink out of the nozzle. The printing parameters from the printer were further tuned to acquire a low thickness while still retaining the pattern shape (see Table 2-1).

Table 2-1: Extrusion printer settings for silver flake ink

Parameter	**Value**
Trace Space (μm)	140
Dispense Height (μm)	60
Print Speed (mm/min)	500
Dispense Pressure (Pa)	250
Relief Pressure (Pa)	75

In preparation for extrusion printing, the tattoo substrate was initially fixed on a glass slide and secured to the printing stage with a set of screws. However, a noticeable amount of unevenness in the substrate was observed causing the printed pattern to vary in ink quantity as the nozzle would print in a concentric format. This was solved by securing only the tattoo paper on the stage with the vacuum on to 80%, to keep the substrate flush against the stage. Below 80%, the substrate would shift when a force was applied by hand. Profilometry scans of the printed square pattern for the tattoo paper secured with the screws and vacuum can be seen in Figure 2-6. A customized PET mask was placed on the stage to prevent excess air from escaping around the substrate with the vacuum on. The tattoo paper was secured onto a glass slide only for inkjet printing.

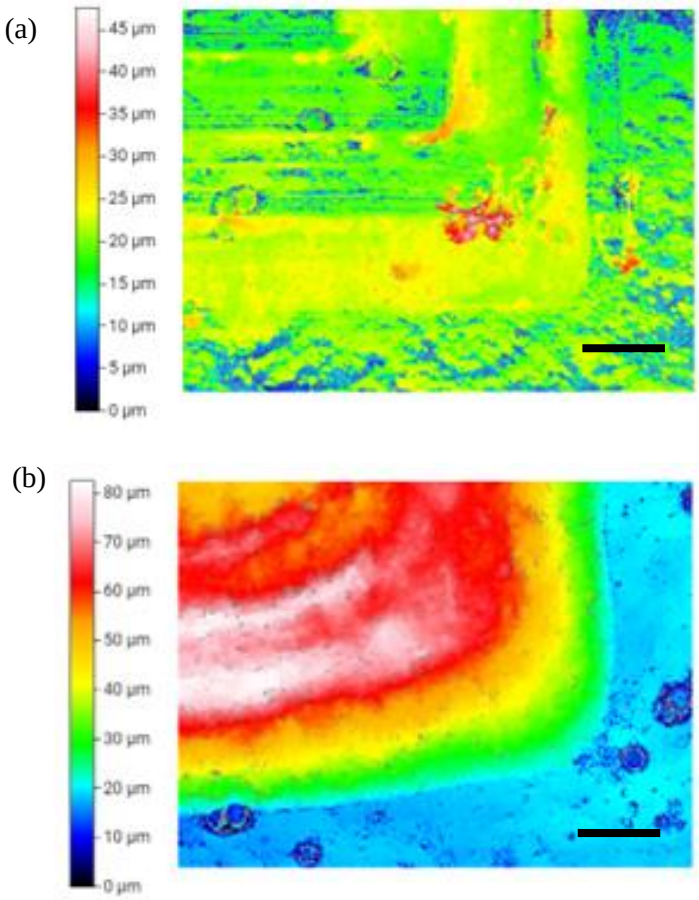

Figure 2-6. Bottom right corner of extrusion printed silver square on printer stage secured with (a) screws, and (b) vacuum. The scale bar indicates 100 µm.

The measured sheet resistance for the extrusion printed electrodes was 10.6 ± 2.0 mΩ/sq for one printed layer. Given that the pattern was visible over the tattoo paper (see Figure 2-6) and the sheet resistance acquired was sufficiently low, only one layer was printed.

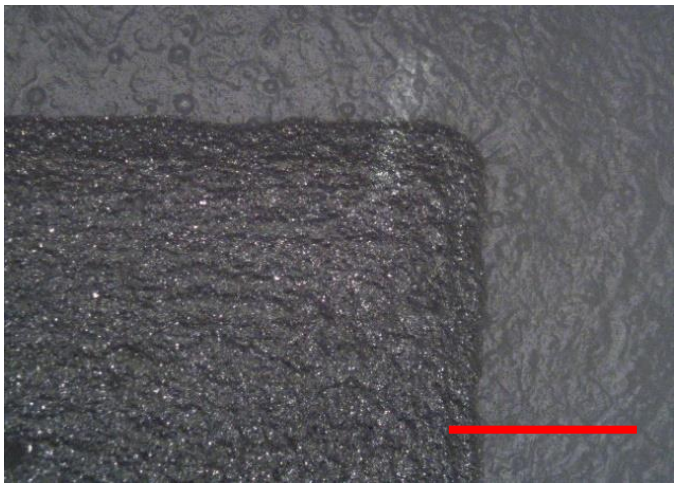

Figure 2-7. Light microscope image of post-annealed silver flake ink square on tattoo paper. The scale bar indicates 1 mm.

Due to the large pore sizes within the tattoo paper (Figure 2-2), which appear to be in the micron range, the silver nanoparticles are susceptible to falling within the pores, causing breaks in the printed pattern. This was remedied by printing multiple layers to fill in the pores and form a more levelled surface. Although the silver flakes are also smaller than the pores, the higher viscosity of the ink allows the ink to sit on top, potentially bridging over the pores.

Both electrodes were dried in a vacuum oven at 100ºC for 30 minutes. Profilometry scans of the top left corners of the inkjet (4 layer) and extrusion printed electrodes can be seen in Figure *2-8*. In addition to its significantly higher thickness relative to the inkjet printed electrode, the extrusion printed electrode shows a more uneven surface profile. The latter observation is attributed to the concentric printing method used to form the square pattern, resulting in more ink near the centre. There was no observed difference between the concentric and raster inkjet printed squares.

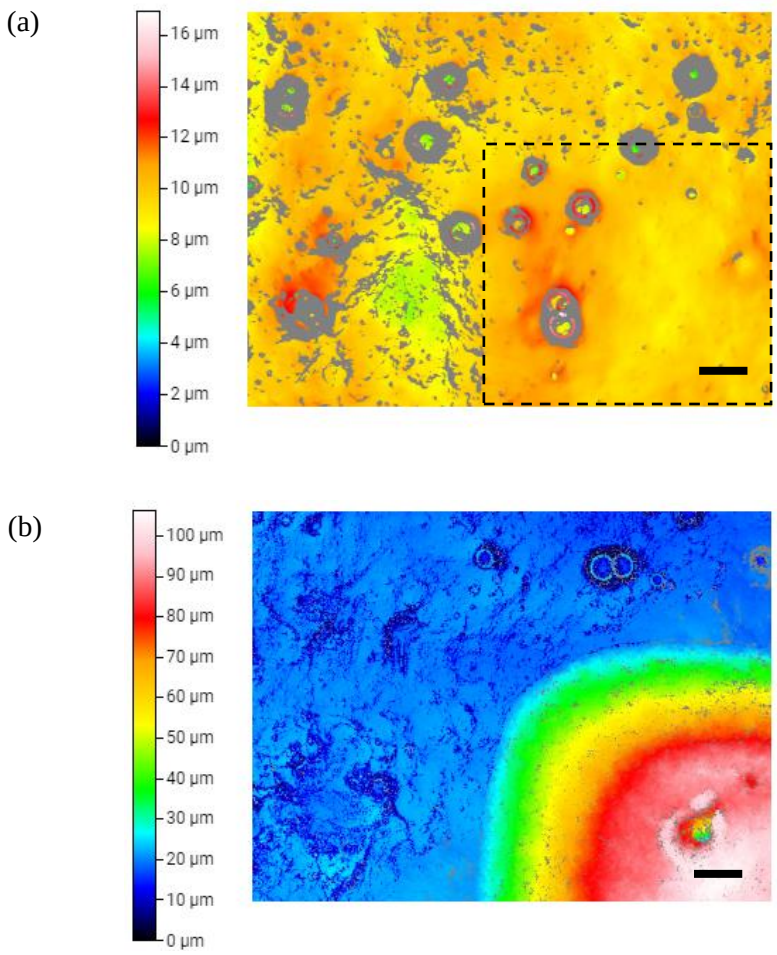

Figure 2-8. Profilometry scans of top left corner of (a) inkjet, and (b) extrusion printed electrodes. The scale bar indicates 100 µm.

Electrodes used for measuring sheet resistance and bending tests were printed alone, while electrodes used for impedance and biophysical signal acquisition included contacts. Extrusion printed contacts (Figure 2-9) were added to the base of the electrode to assist with connections to external hardware. Note the extrusion printed electrodes were printed directly with the contacts.

(a) (b)

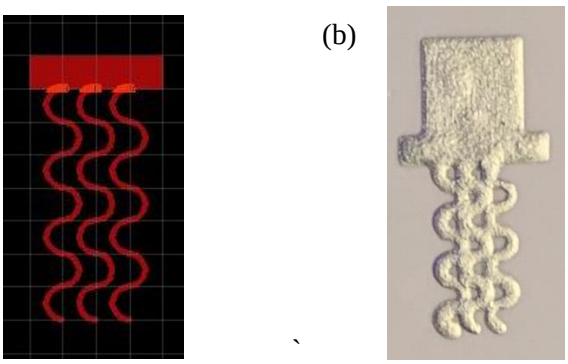

Figure 2-9. (a) EAGLE design of tattoo contact, and (b) Contact printed with extrusion printed square electrode. Note the rectangle in the contact is 1 mm wider on each side.

During the inkjet printing process of the spiral matrix, the stage was heated. Even with a heated stage during printing, which would dry the edges of the printed line, the pattern definition of the spiral matrix was not perfectly retained. This can be attributed to the random sizes and distribution of pores in the paper that causes the ink to spread outside the printed line. A side-by-side view of the inkjet and extrusion printed electrodes can be seen in Figure 2-10.

(a) (b)

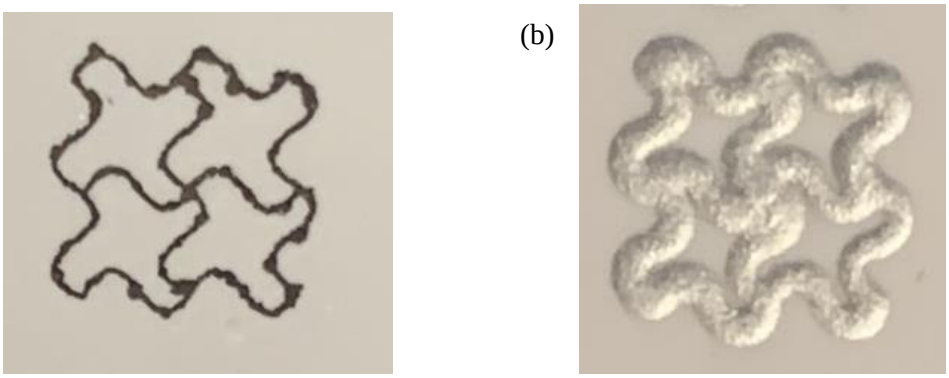

Figure 2-10. Spiral matrix formed using (a) inkjet, and (b) extrusion printing

For the inkjet printed electrodes, additional flash sintering was performed with a xenon lamp (X-1100, XENON Corporation, Wilmington, MA) using experimentally derived parameters discussed further in the following section.

2.3. Effect of Post-Annealing Parameters on Sheet Resistance

The post printing treatment was optimized for each fabrication method. To obtain sufficient sintering of the inkjet printed silver nanoparticles, thermal and flash (IPL) sintering parameters were varied. For thermal sintering, the drying time was varied from 30, 60, and 90 minutes at 100ºC (a temperature suitable for the given substrate). As shown in Figure 2-11, there was no significant improvement in the resulting sheet resistance with a longer drying time, so the final drying time chosen was 30 minutes. The IPL settings used were at 2000 V, with an ON time of 1 ms and OFF time of 10 ms, and a variable number of pulses applied.

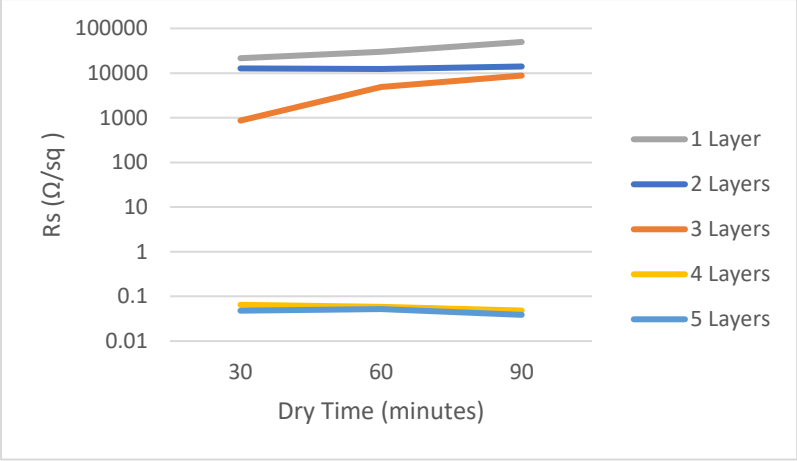

Figure 2-11. Change in sheet resistance for different number of printed layers with respect to drying time. Note that the samples were only dried post-printing.

SEM images for 1-to-5-layer samples can be seen in Figure 2-12 . With an increase in ink layers, there is no noticeable change in the distribution or behaviour of the nanoparticles on the nanoscale.

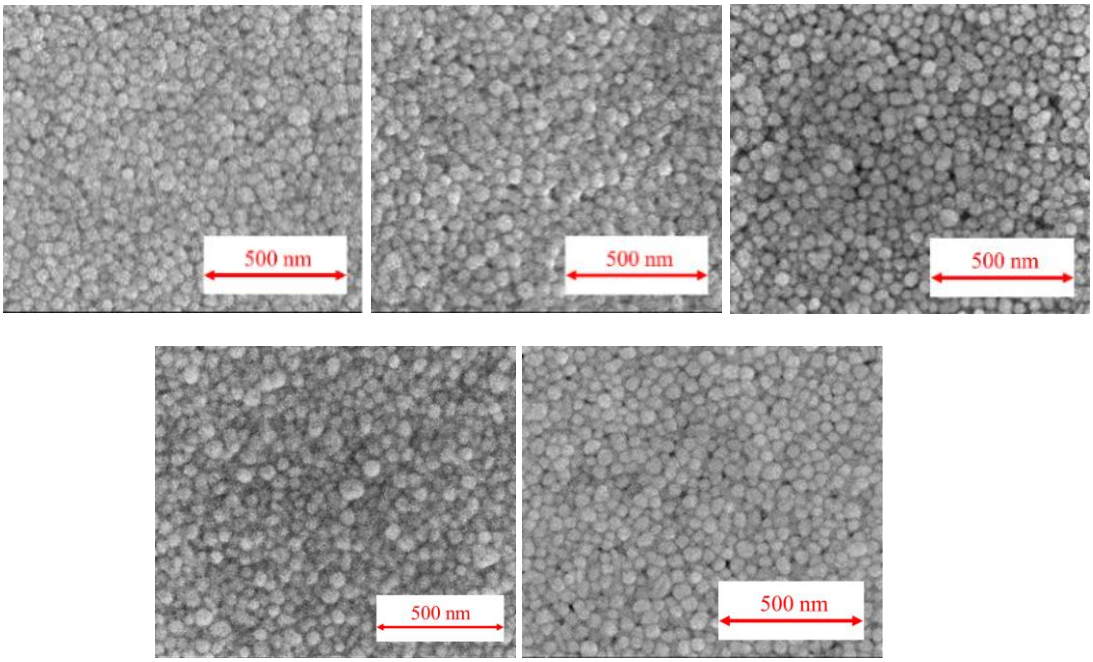

Figure 2-12. SEM images of 1 (top left) to 5 (bottom right) dried AgNP layers on tattoo paper

Ultimately, the final sheet resistances for the extrusion and inkjet printed electrodes, 10.6 ± 2.0 mΩ/sq and 35.4 ± 2.49 mΩ/sq were comparable to the screen-printed Ag/AgCl electrodes mentioned previously [45]. Although a low sheet resistance is not necessarily needed for medical tattoos to function, as evidenced with the graphene-based electrodes mentioned [9], a lower Rs value potentially reduces the impedance of the electrodes, which enhances the sensitivity to ionic potentials reaching the skin.

2.3.1. IPL for Inkjet Printed Electrodes

IPL settings including applied voltage, ON/OFF time and number of pulses were selected experimentally, to acquire sufficient sintering with the least amount of microscopic damage to the sample. An application of a potential higher than 2000 V resulted in complete delamination of the printed pattern. The use of a ratio higher than 1 to 10 for ON to OFF time also resulted in apparent damage.

The number of IPL pulses for the inkjet printed electrodes were incremented by 2, with the sheet resistance measured after each application of flash sintering. Figure 2-13 shows the change in sheet resistance with a gradual number of applied pulses for electrodes with varying layers. As seen, even a low sheet resistance of 53.9 ± 6.0 mΩ/sq for 2 printed layers is acquired after applying 4 pulses.

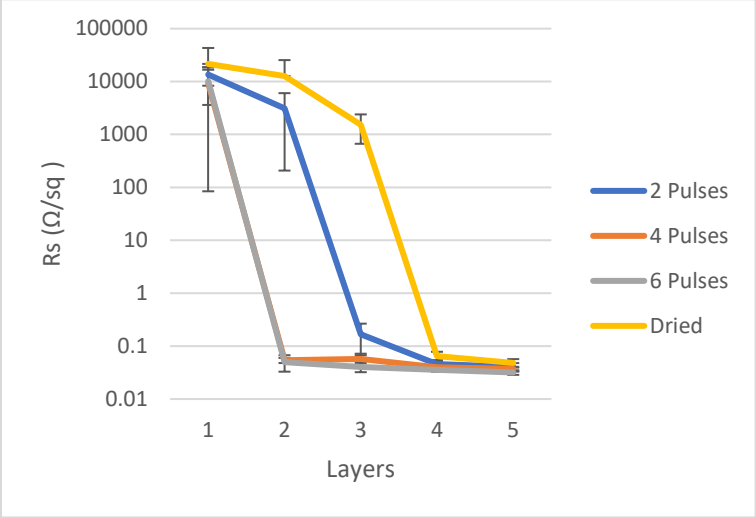

Figure 2-13. Change in sheet resistance with 2, 4, and 6 IPL pulses applied to inkjet printed electrodes with 1 to 5 layers

Based on the SEM images taken, there was a notable improvement in nanoparticle sintering after applying only 6 IPL pulses. As seen in Figure 2-14, the silver nanoparticles demonstrate signs of necking and merge with the application of more pulses to form a conductive film.

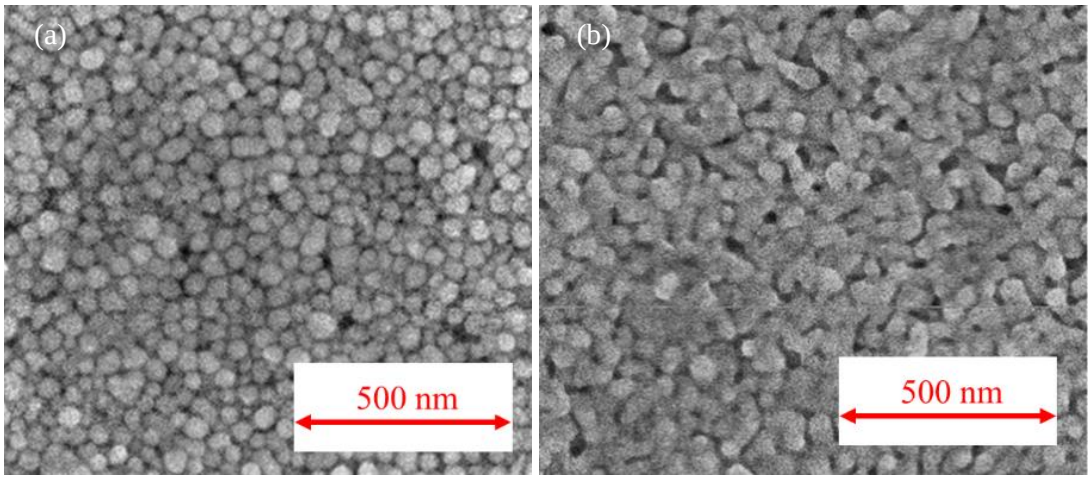

Figure 2-14. SEM images of 3 layer (a) dried and (b) dried with 6 IPL pulses applied electrodes on tattoo paper

Given that the sheet resistance was significantly reduced with six IPL pulses, as shown in Figure 2-15, this quantity of pulses was applied to the printed electrodes to improve the electrical performance.

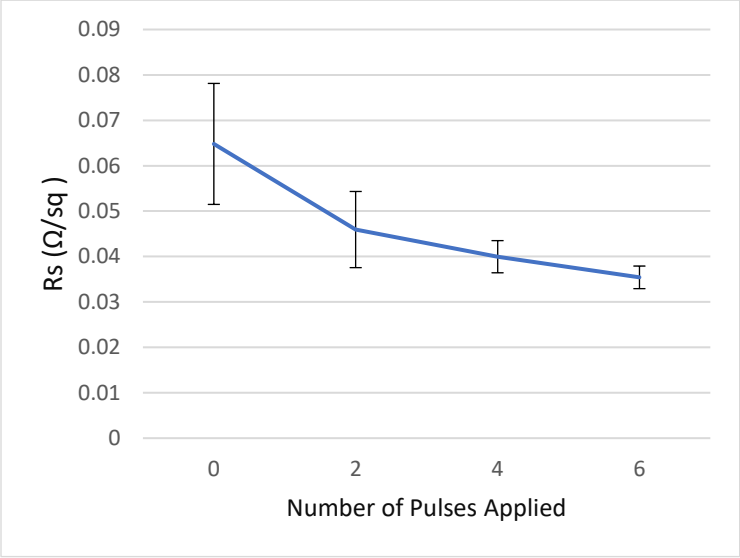

Figure 2-15. Change in sheet resistance with 0 (dried), 2, 4, and 6 IPL pulses applied to inkjet printed electrodes with 4 layers

2.4. Conclusion

In summary, the fabrication process of the inkjet and extrusion printed tattoo electrodes was completed and studied, and further characterization of the materials used was performed. Inkjet and extrusion printing processes were optimized to form the complete silver patterns on tattoo paper containing minimal defects. The porous nature of the tattoo paper substrate used presented a challenge when inkjet printing, thus requiring additional steps such as printing multiple layers and using flash sintering post fabrication. Although simpler, the extrusion printing process yielded patterns that were thicker compared to those that were inkjet printed. The sheet resistance values of the tattoo electrodes are comparable and on the lower end of the values reported in the literature for electrodes developed with different materials and fabrication processes [9]. The tuning of the printing processes allows for further potential to print more complex patterns on tattoo paper for other biomedical applications beyond biophysical signal acquisition.

CHAPTER 3. TATTOO ELECTRODE PERFORMANCE

3.1. Introduction

Performance evaluation of medical sensors is a vital step during their fabrication/development process. When gathering information pertaining to the efficacy of the biophysical sensors in an in vitro environment, mechanical and electrical stability are critical metrics to examine. This will ensure success during in vivo testing and reliability during long term use.

Phantom models are a common tool used during the development of bioinstrumentation devices/sensors as they allow for controlled, in vitro testing. These models are commonly formed with a gelatin-like material to suspend a charge carrying material such as sodium chloride (NaCl) [48]. The concentration of NaCl can be modified to change the conductivity of the model, potentially forming a conductivity close to the human body. An electrode can be placed within the model to emit a signal that can be received by an electrode placed outside the model. This methodology has been previously demonstrated to examine the performance of an array of printed PEDOT:PSS tattoo electrodes to assess how effectively they can collect square wave signals, as shown in Figure 3-1 [8]. Simulating electrodes are placed on the base of the phantom model, and the simulated signal is collected by Ag/AgCl and tattoo electrodes on top to compare the performance of the microfabricated and conventional electrodes.

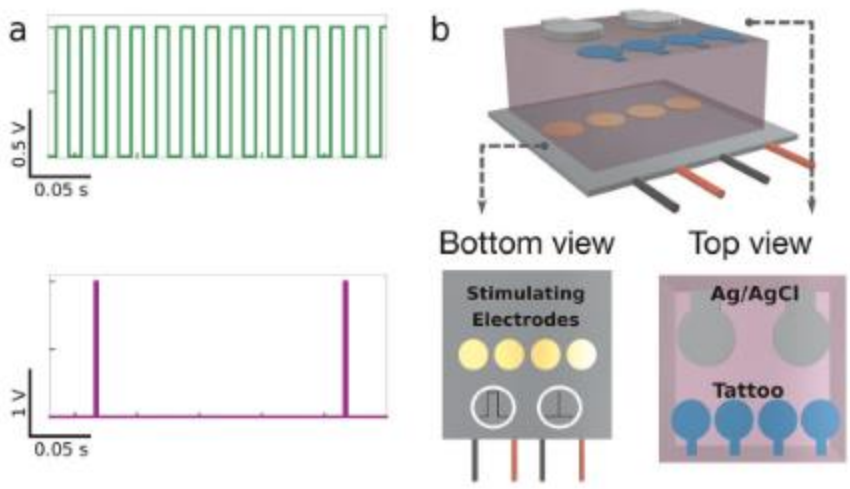

Figure 3-1. Performance measurement setup for PEDOT:PSS tattoos. Reproduced with permission [8]. Copyright © 2020, Springer Nature Publishing Group

The impedance measurements of previously reported electrodes have been acquired in an in vivo setting. At the lower frequency range (0.1-50 Hz), previously reported electrodes have an impedance one to two orders of magnitude [9] higher than the commercial Ag/AgCl electrodes. Past the lower frequency range, the tattoo electrodes approach the impedance of commercial electrodes.

A notable challenge when integrating skin conforming sensors to rigid signal collecting electronics is the intermediate contact between the two components [8]. Contacts currently implemented to work with medical tattoos tend to be complex and do not perfectly conform to skin like the tattoo.

3.2. Experimental

To acquire impedance measurements of the electrodes, a phantom model was fabricated. The phantom model was made by combining 15 g of gelatin (ClassiKool 240 Bloom Gelatine, UK), 1 g of NaCl (Fisher Scientific), and 50 mL of deionised water, stirred and heated at 60 ^{o}C for 15 minutes to dissolve the granules in the mixture. The mixture was subsequently poured into a 3D

printed polylactic acid (PLA) mold (6 mm × 6 mm × 2 mm). A metal cup electrode (Grass Disposable Deep Cup Electrode Ag/AgCl) was secured to the base of the mold. It was cured in the refrigerator for 24 hours. The model was left at room temperature for 20 minutes prior to conducting impedance measurements.

Impedance measurements were conducted using a potentiostat (Metrohm Autolab PGSTAT204 Compact and modular potentiostat/galvanostat). A cross section of the printed electrode (representative of the inkjet or extrusion printed electrodes) on the phantom model can be seen in Figure 3-2. Conventional electrodes (3M 2560 Red Dot Multi-Purpose Monitoring Electrode) were used for comparison purposes.

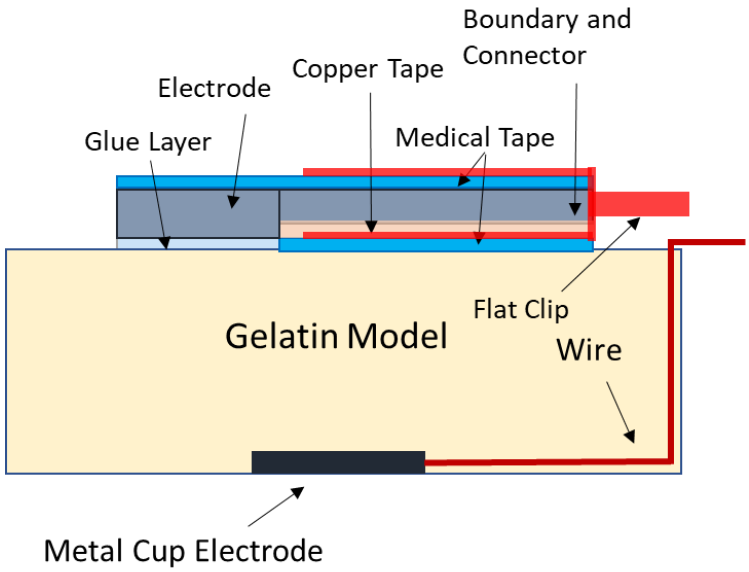

Figure 3-2. Cross sectional view of tattoo on phantom model

The electrical performance of the electrodes with the application of bending strain was also examined. Dowels with radii of 25 mm, 20 mm, 15 mm, 10 mm, 7.5 mm, and 4 mm were designed in Fusion 360 and 3D printed (Ultimaker) using PLA. The square electrodes were cut out and placed on the dowels, from largest to smallest bending radii, and the resistances were measured using the same 4-point probe method previously used to measure sheet resistance.

A simple contact platform was developed to connect the soft medical tattoos to external biomedical circuitry (see Figure 3-2 for an illustration and Figure 3-3 for an image). The objective of the contact is to allow a rigid component to connect to the electrode without coming in contact with the skin or phantom surface and causing no damage to the tattoo. This setup enables measurement of only the ionic behaviour from the electrode itself. The contact, which is composed of an extrusion printed pattern on a small piece of copper tape, is be placed between two pieces of medical tape to maintain the integrity of the tattoo during measurements. A flat clip is used to connect to the contact.

Figure 3-3. Extrusion printed square electrode with contact (highlighted) on human participant

3.3. Impedance Tests

The impedance and the impedance normalized by contact area was measured from 0.1 Hz to 1,000 Hz, with the results shown in Figure *3-4* and Figure 3-5 respectively. When examining the impedance alone, the impedance of both inkjet and extrusion printed tattoos is higher than that of the conventional electrode. However, when taking the sizes of the electrodes into account, the impedance of the extrusion printed tattoo becomes lower than the conventional electrode. The sizes of the electrodes, 16 mm^2 for the printed electrodes and 78 mm^2 for the conventional electrode,

were accounted for by multiplying impedance with electrode area. As seen in the plots, the extrusion printed electrodes possess a lower impedance and a smaller error range (illustrated by the shaded region) at low frequencies compared to the inkjet printed electrodes, while the conventional electrodes maintain a low and consistent impedance over the frequency range.

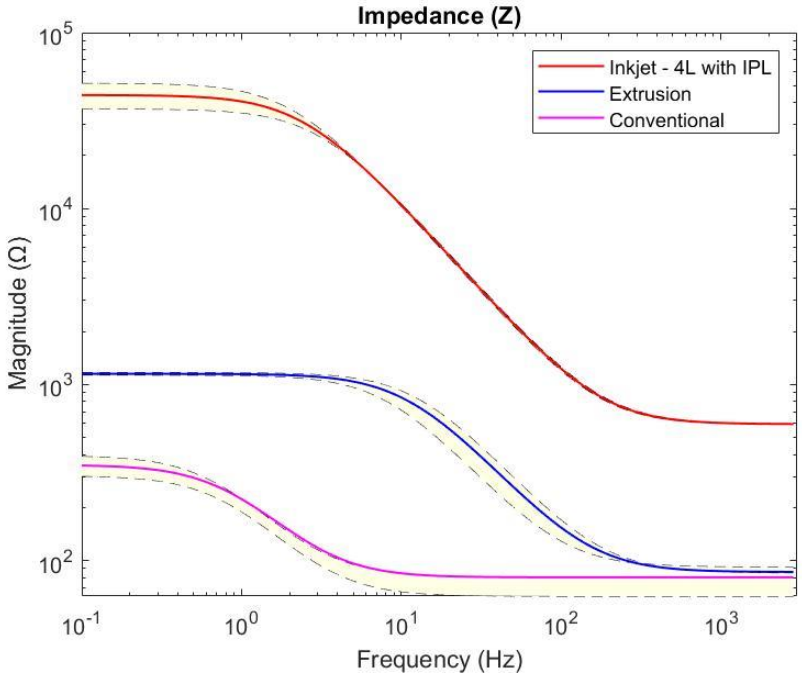

Figure 3-4. Impedance of inkjet printed and extrusion printed square tattoo electrodes, and conventional electrodes

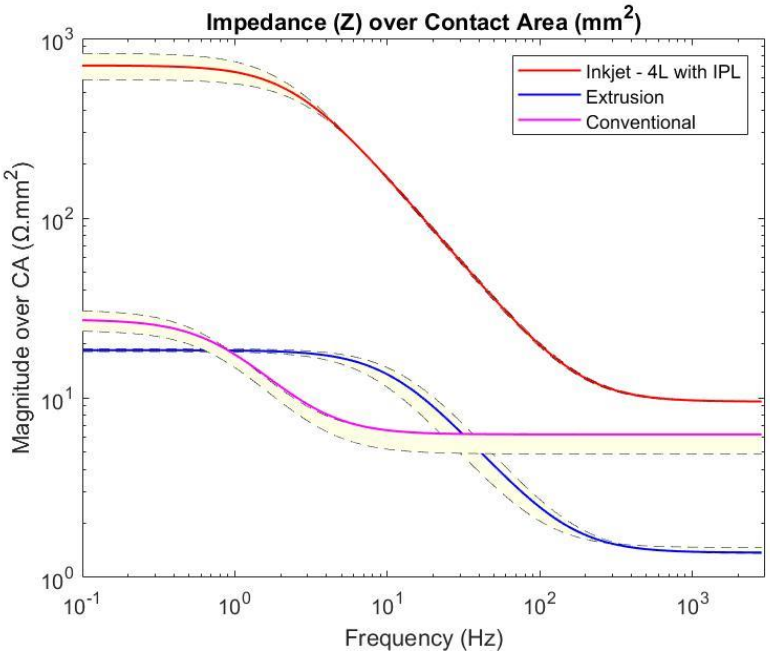

Figure 3-5. Impedance of inkjet printed and extrusion printed square tattoo electrodes, and conventional electrodes over contact area (mm^2)

An equivalent circuit model can be used to represent the skin-electrode impedance. Within the model, parallel components Rd and Cd represent impedance at the electrode-electrolyte interface and Rs, which is the resistance of the actual electrode materials that is in series with Rd and Cd [35]. Since the extrusion printed electrodes are not partially absorbed into the tattoo paper like the inkjet printed electrodes, there is likely a larger contact area of conductive material to the gelatin model at the tattoo-phantom interface, resulting in a lower value for Rd and higher value for Cd. The equivalent circuit models of the inkjet and extrusion printed electrodes can be seen in Figure 3-6.

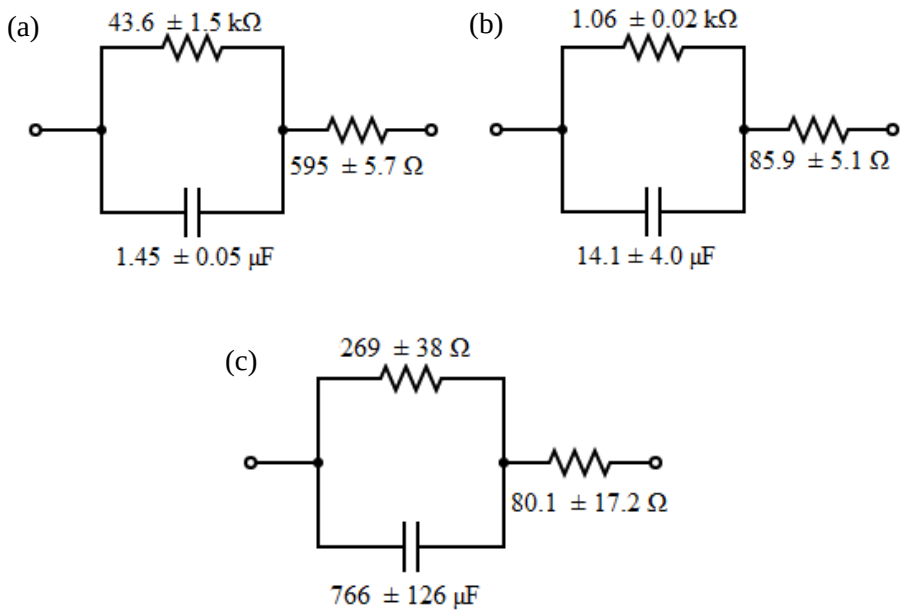

Figure 3-6. Equivalent circuit model of electrode-phantom interface for (a) inkjet and (b) extrusion, and (c) conventional electrodes

Overall, the extrusion printed electrodes perform better than the inkjet printed electrodes, as the impedance is lower at the lower and higher frequency ranges. The cut-off frequency for the extrusion printed electrode (10.65 Hz) is larger than that of the inkjet printed electrodes (2.52 Hz), enabling the electrode to perform over a wider range of frequencies more effectively. Although the tattoos had a higher impedance compared to a conventional electrode in the lower frequency range, their behaviour was more stable in this range. For the acquisition of medical signals, this would be beneficial as these signals can go up to almost 100 Hz [49].

3.4. Bending Tests

Bending tests for microfabricated components can be reliably conducted with the use of dowels, which bend the sample at a certain bending radius given by the radius of the dowel. shows

the formula for the bending curvature, showing that the bending curvature is inversely proportional to the radius of the dowel used.

$$Bending\ Curvature\ \left[\frac{1}{mm}\right] = \frac{1}{Dowel\ Radius\ [mm]} \qquad \text{Equation 3-1.}$$

Uniaxial bending tests for the tattoo electrodes were conducted, with the change in resistance measured during each applied bending radius. The results of the bending experiments, as seen in Figure 3-7, indicate that the inkjet and extrusion printed electrodes perform similarly down to a certain bending radius. Once the inkjet printed electrodes reach a bending curvature of 0.2/mm, the resistance increases significantly. The inkjet printed electrode exhibited cracking at a smaller bending radius, which contributed to the progressive increase in resistance. Conversely, the extrusion printed electrodes maintained a generally consistent performance as more strain was applied. There was also a lower error overall for the normalized resistance for the extrusion printed electrodes, compared to their inkjet printed counterparts. The resistance returns to the initial value after each bending test. Due to the rigidity of the silver component in the conventional electrode, the bending results for these electrodes were not included.

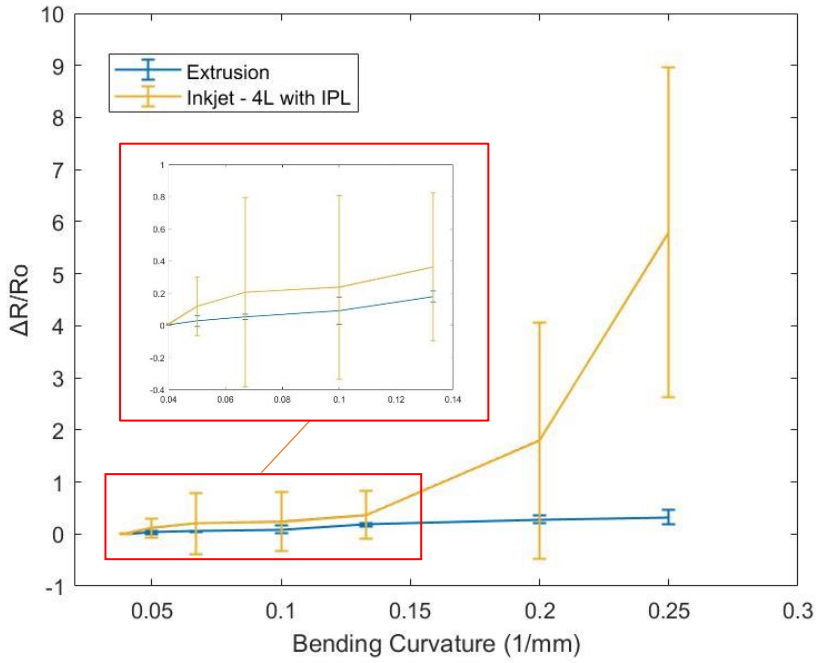

Figure 3-7. Normalized resistance as a function of bending curvature for inkjet and extrusion printed electrodes

3.5. Mechanical Performance of Spiral Matrix Tattoo Electrodes

In addition to the inkjet and extrusion printed squares, other shapes including circles and spiral matrices were also printed and tested. The objective of printing different shapes was to primarily compare the mechanical performance of the different geometries. Given that a serpentine shape is known to be more flexible compared to a straight line, as its longitudinal component and offset component (which is at an angle to the longitudinal component) can maintain its structure while being stretched along the longitudinal axis [50], a serpentine shaped/ spiral matrix was formed and compared to the initial square shape tested. The spiral matrix would allow the electrode to withstand biaxial stress, which would be useful when the electrode is placed on the skin and potentially subjected to stress along two planes.

Figure *3-8* shows the change in sheet resistance with respect to bending radius for the inkjet and extrusion printed square and spiral matrix electrodes. In the case of the extrusion printed electrodes, the change in resistance for the squares becomes increasingly higher than that of the spiral electrodes. Neither of the shapes experience failure at a higher bending radius. For the inkjet printed electrodes the square experiences failure when the bending curvature is greater than 0.133/ mm, while the spiral matrix maintains a steady performance over all the bending curvatures.

(a)

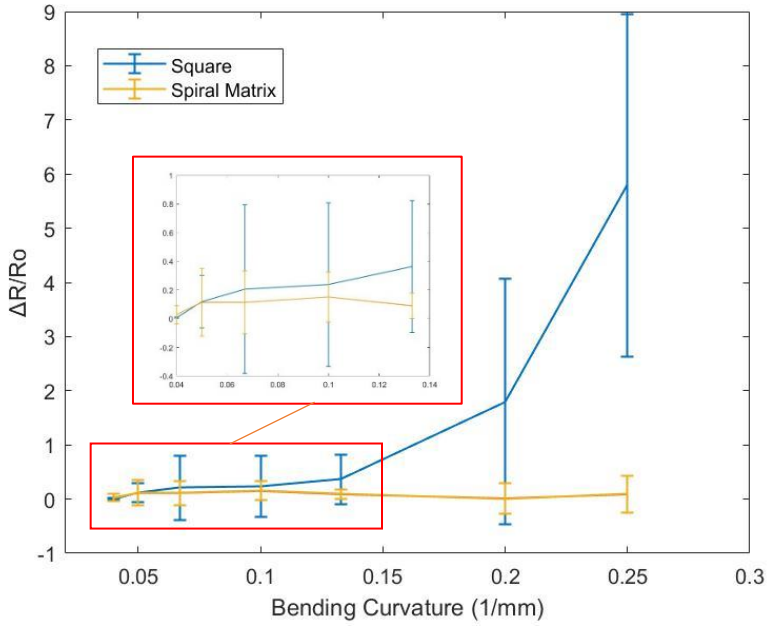

(b)

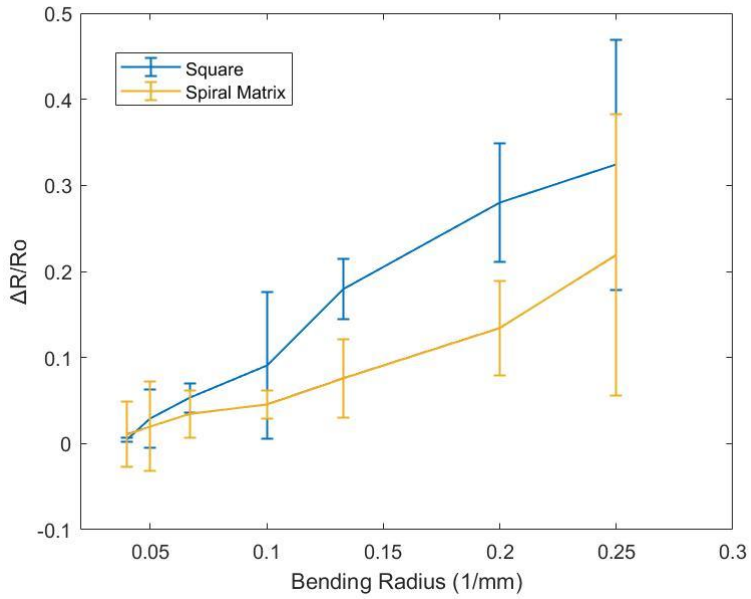

Figure 3-8. Change in bending resistance of square and spiral matrices fabricated using (a) inkjet, and (b) extrusion printing

3.6. Conclusion

The electrical and mechanical performance of the inkjet and extrusion printed tattoo electrodes are examined and compared in an in vitro context. A phantom model was developed and implemented in the analysis of the impedance of the electrodes over a range of frequencies. Compared to the extrusion printed electrodes, the inkjet printed electrodes had a higher impedance and greater error range. Bending tests for the tattoo electrodes were also performed, comparing inkjet and extrusion printed squares, as well as squares and spiral matrices printed using each method. Overall, the extrusion printed electrodes maintained a constant sheet resistance over a range of bending radii, with the spiral matrix exhibiting the best performance.

CHAPTER 4. TATTOO ELECTRODES FOR BIOPHYSICAL SIGNAL ACQUISITION

4.1. Introduction

Acquisition of electrophysiological signals can provide further insight into the functionality of physiological systems in the human body. The components that are used to measure these signals, including the skin-interfacing electrodes/sensors and data acquisition system, must be as robust as possible. The former components are particularly important to optimize as they largely determine the quality of the signals and potentially prevent the need for further processing.

EMG tests record the electrical activity of skeletal muscles in the body which originate from motor neurons causing muscles to contract [68]. These tests are conducted to determine whether an individual has a muscular/neural condition such as muscular dystrophy, carpal tunnel syndrome, and amyotrophic lateral sclerosis [68]. In addition to diagnostic purposes, EMG signals can also serve a functional purpose to control components such as prosthetics [69]. Medical electrodes are connected depending on the target area of the condition, but are generally placed on the arm or leg.

Conversely, ECG tests record the electrical activity of the heart, and are conducted to diagnose problems in the heart such as cardiac arrythmias and coronary artery disease [51]. These tests are taken by attaching up to 12 electrodes on the chest and limbs, and the electrodes deliver the data to a data acquisition system to process and display the data [51]. A simple method used to connect the electrodes is with the Einthoven triangle format, named after the Dutch physician Willem Einthoven [53], as shown in Figure 4-1. This method only requires three electrodes that are connected to the right arm, left arm, and left leg, which form three bipolar leads (I, II, and III). These leads form a graph that displays the potential difference between two limbs, with lead II being equal to the sum of leads I and III according to Einthoven's law [52]. Typically, the patient is supposed to lie still to prevent any artifacts in the signals [51].

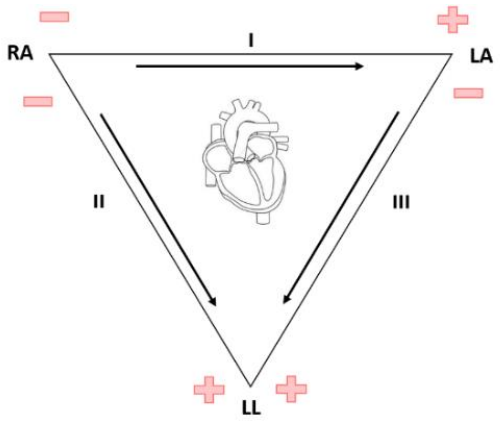

Figure 4-1. Einthoven triangle for ECG signal acquisition. RA denotes right arm, LA denotes left arm, and LL denotes left leg. [52]

The resulting structure of an ECG waveform can be seen in Figure 4-2. Each component of the waveform represents a specific action occurring as blood moves into and out of the heart. The P wave represents depolarization of the atria (plural for atrium, which is the upper chamber of the heart) [54]. The QRS interval includes three waves and represents depolarization of the ventricles, which are the lower chambers of the heart [54]. Lastly, the T wave represents repolarization of the ventricles [54].

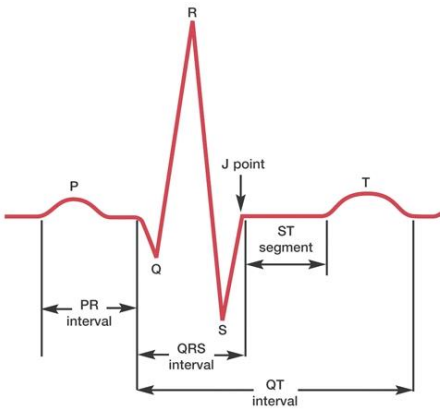

Figure 4-2. Labelled ECG waveform [54]

4.2. Experimental

ECG signals were acquired using a Biopac MP36 Data Acquisition (DAQ) Unit (Biopac Systems Inc., USA), which collected and applied additional filtering to the signals. Selected specifications of the Biopac DAQ Unit can be seen in Table 4-1.

Table 4-1. Biopac MP36 DAQ Unit specifications

Specification	**Value**
Number of Channels	4 Channels
A/D Sampling Resolution	24-bit
Input Voltage Range	Adjustable from ± 200 μV to ± 2 V
Input Noise Voltage	9 nV rms /sqrt (Hz) and 0.1 μV rms noise (0.1 Hz to 35 Hz) - nominal
Common Mode Rejection Ratio (CMRR)	85 dB minimum

The conventional electrodes (3M 2560 Red Dot Multi-Purpose Monitoring Electrode) and tattoo electrodes were connected to channel 1 and 2 of the unit respectively, with a lead set. The electrodes were connected side by side (see Figure 4-3 for example) on the right arm, left arm, and left ankle, based on the Einthoven triangle to record the ECG signals. To collect the EMG signals, two electrodes were placed on the participant's wrist (one for ground and one for Vin+) and another electrode was placed further down the arm near the cubital fossa or elbow pit (for Vin-). The electrodes were placed on the participant's dominant arm. Three healthy subjects, two females and one male aged between 23 and 33, participated in the experiments conducted. To record the ECG signals, he subjects were told to sit still for one minute to record the signals. To record the EMG signals, the participant held a stress ball and would rest for two seconds and squeeze the ball for two seconds.

Figure 4-3. Extrusion printed circle electrode with contact and conventional electrode on left arm

Impedance tests were conducted on one female subject aged 23 using a potentiostat (Metrohm Autolab PGSTAT204 Compact and modular potentiostat/galvanostat), used previously to take in vitro tests with a phantom model. To conduct the measurements, a conventional electrode was placed on the right leg for grounding, and the conventional and tattoo electrodes were placed side by side on the right arm for comparison purposes.

Hardware based processing of the signals acquired was completed with the Biopac DAQ unit. Low pass (20 kHz) and high pass (0.05 Hz) filters were used to remove noise and external (i.e. powerline) interference. Software based filters used in the corresponding Biopac computer application included three automatic programmable digital (infinite impulse response (IIR)) filters. Additional filtering was conducted in MATLAB 2021b to examine the quality of the resulting signals and calculate SNR.

4.3. Electrophysiological Signal Results

The ECG results using conventional and square (inkjet and extrusion printed) electrodes from the male and female participant can be seen in Figure 4-4. The signals shown are plotted without additional filtering to examine their raw behaviour. The signals acquired from tattoo electrodes are nearly identical to those acquired with the conventional electrodes. It is of note that the amplitude of the QRS complex within the ECG signals collected with the inkjet printed electrodes is smaller than that of the other electrodes. This can be due to the higher impedance of the inkjet printed electrode, reducing the ability for the electrode to strongly sense the heart activity.

(a)

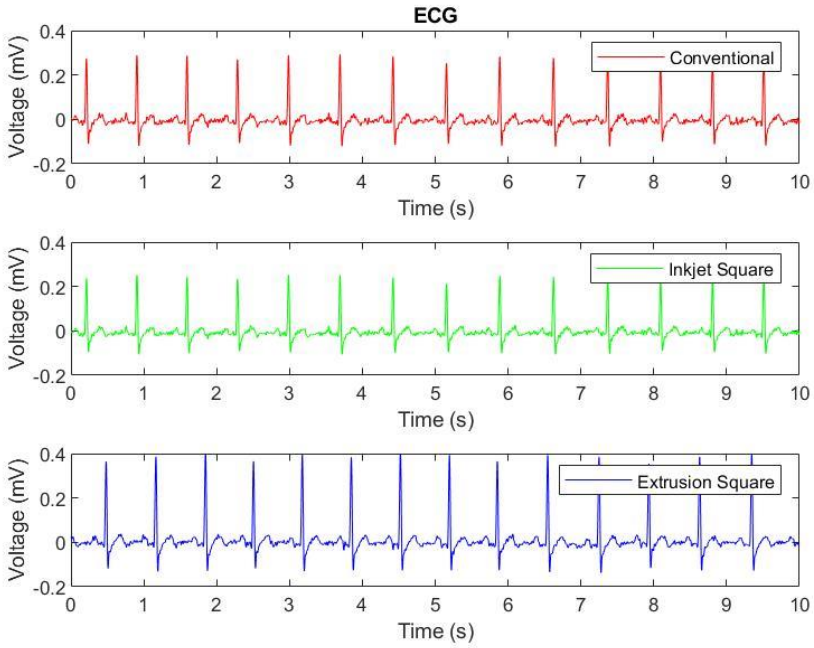

(b)

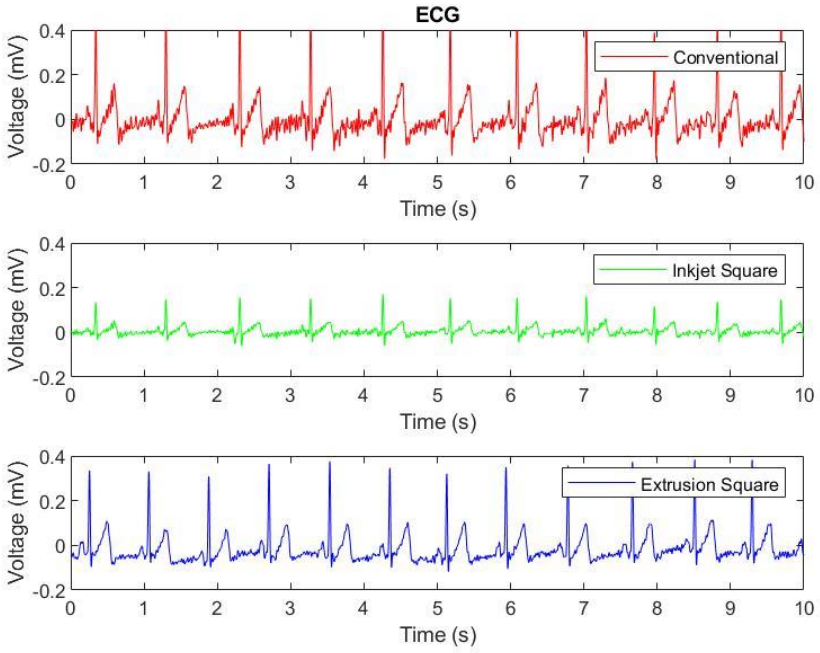

Figure 4-4. ECG results with inkjet printed square electrode, extrusion printed square electrode, and conventional electrode on (a) male, and (b) female participant

While the general structure of the ECG waveforms between the male and female participant was the same, the signals taken with the tattoo electrodes from the male participant had a QRS complex with a larger amplitude. This is often the case in signals acquired from men, as they possess a larger cardiac mass and higher left ventricle wall thickness [55].

EMG signals were also acquired and compared. A 20 second window of the signals obtained with conventional, extrusion and inkjet printed square electrodes can be seen in Figure 4-5. The signals acquired with the extrusion printed electrodes were comparable to the conventional electrode in terms of noise and signal amplitude. Conversely, the inkjet printed electrodes yielded more noise as shown during the relaxation periods, and the EMG signals showed a characteristic peak at the start and end of the signal.

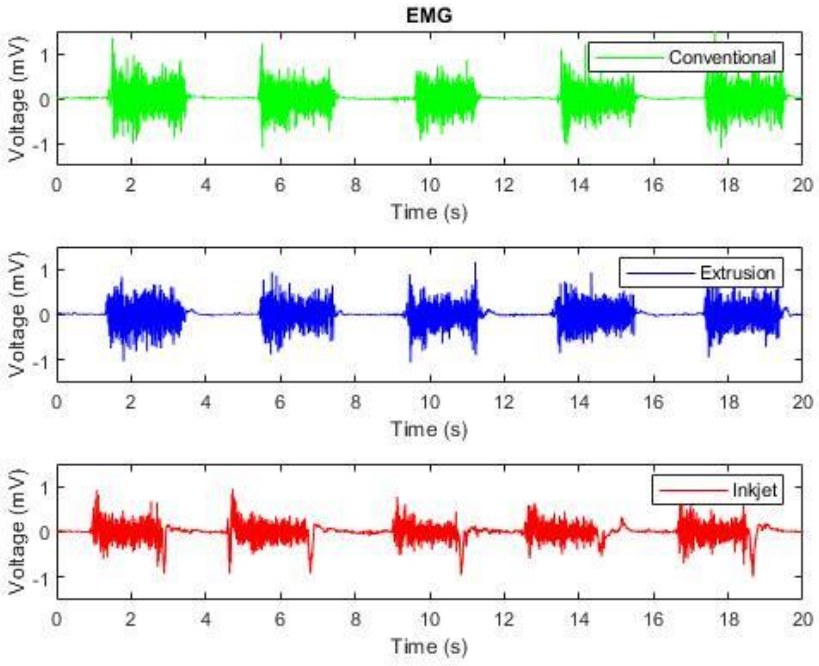

Figure 4-5. EMG results with conventional, inkjet square, and extrusion square electrodes from female participant

4.3.1. Performance of Different Electrode Shapes

The different electrode shapes, as seen in Figure 4-6 were tested on the participants. The ECG signals acquired with these electrodes can be seen in Figure 4-7. For the inkjet printed electrode, the circle electrode showed the least amount of noise within the signal. Of the extrusion printed electrodes, the signal from the square electrode showed the least noise and clearly showed the different waves present in the signal. Overall, there were no significant differences between the shapes printed and the appearance of the ECG waveforms.

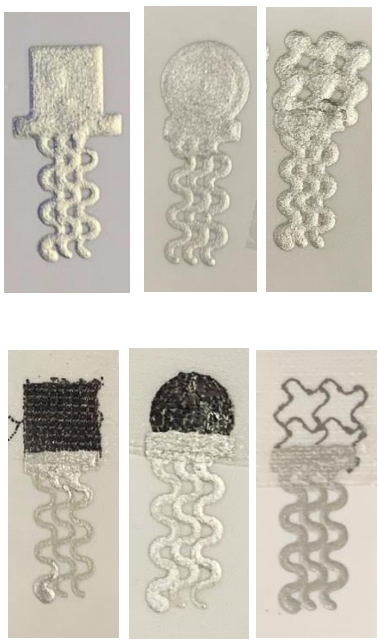

Figure 4-6. Extrusion (top row) and inkjet (bottom row) printed squares, circles, and spiral matrices

(a)

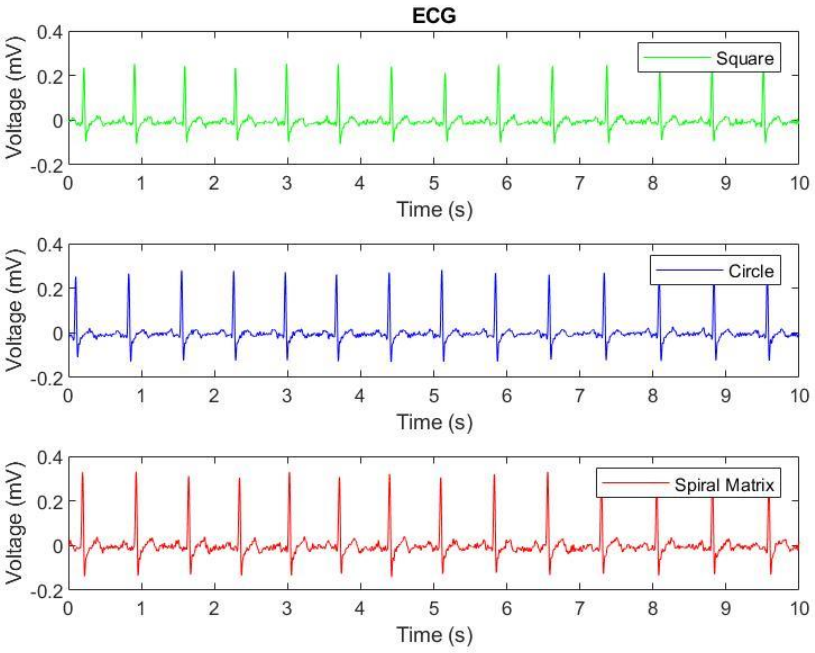

(b)

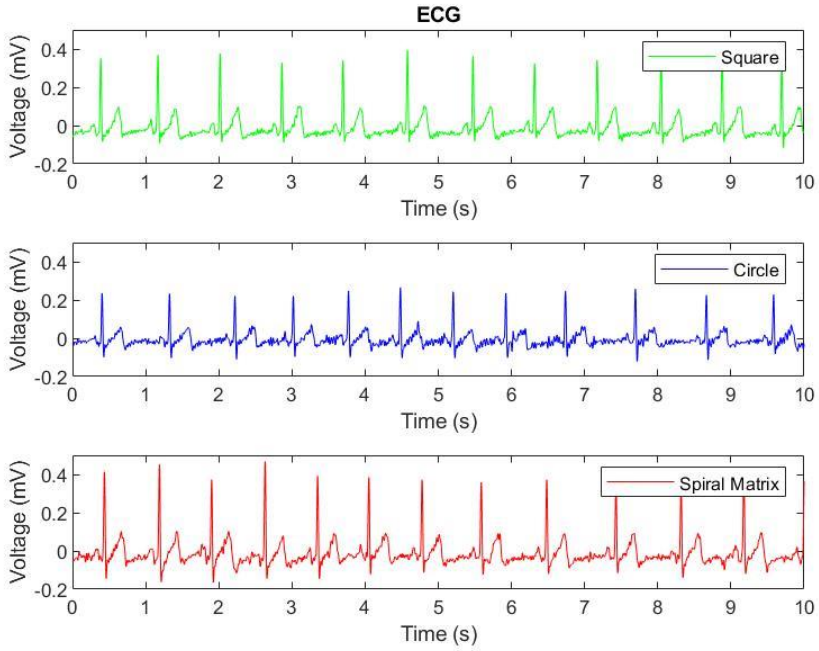

Figure 4-7. ECG results with different (a) inkjet printed and (b) extrusion printed electrode shapes (square, spiral, and circle) from male participant

Additional EMG signals recorded with the square, circle, and spiral shaped extrusion and inkjet printed electrodes can be seen in Figure *4-8*. All the inkjet printed electrodes produced signals with greater instability and characteristic spikes at the start and end of the EMG signal. The inkjet printed spiral matrix yielded the worst signal. Comparing the extrusion and inkjet printed electrodes, the inkjet printed electrodes did not perform as well. Since the EMG signals are of a higher voltage compared to the ECG signals (at ~ 1 mV compared to ~0.2-0.5 mV), the inkjet printed electrodes would not perform as robustly due to a higher resistance and thus, higher impedance.

(a)

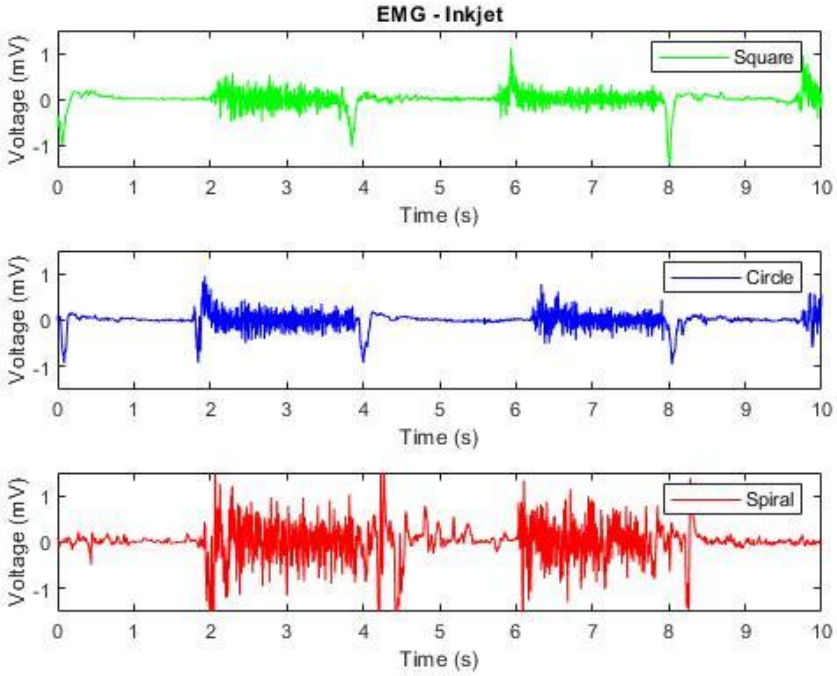

(b)

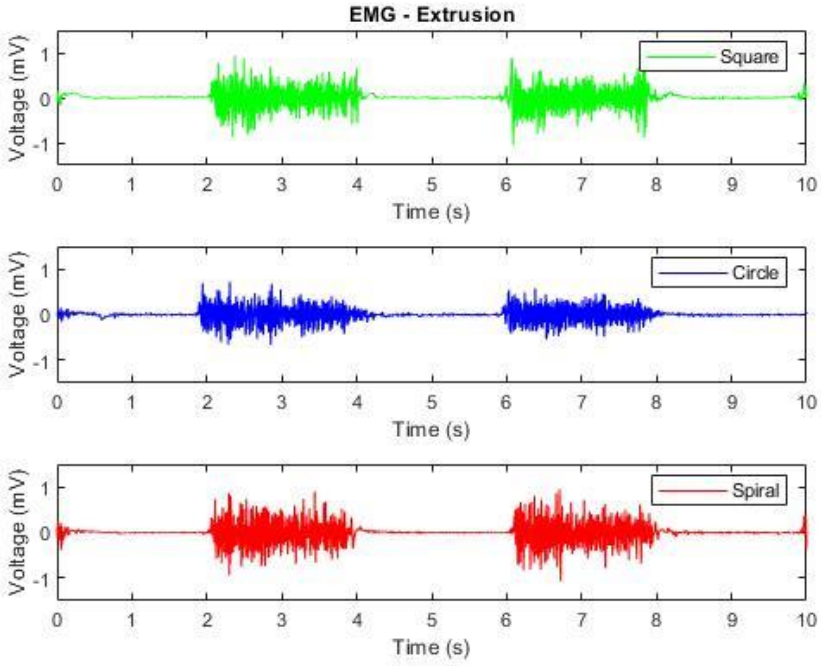

Figure 4-8. EMG results with different (a) inkjet printed and (b) extrusion printed electrode shapes (square, spiral, and circle) from Female participant

4.3.2. Signal Analysis

Further analysis of the signal quality was conducted through the acquisition of the signal-to-noise ratio (SNR) using the EMG signals obtained. Several methods have been reported to find the SNR for these signals. In one method, the SNR represents the ratio between summed squared magnitudes of the wanted signal and the noise present within the signal [56] (see Equation 4-1). Alternatively, the SNR can be found by dividing the standard deviation of the noise by the peak value of the power signal [62] (see Equation 4-2). The first method was primarily used for the analysis of the individual electrode shapes.

$$\text{SNR (dB)} = 20\ log_{10}\left(\frac{\sqrt{(\sum VSignal^2)}}{\sqrt{(\sum VNoise^2}}\right) \qquad \text{Equation 4-1 [56]}$$

$$\text{SNR (dB)} = 20\ log_{10}\left(\frac{MaxVSignal}{\sigma VNoise}\right) \qquad \text{Equation 4-2 [62]}$$

To calculate the SNR, the initial signal was loaded into MATLAB 2021b and one second segments with the arm at rest were used as the noise signal and one second segments where the participant applied a clenching force were used as the power signal.

The resulting SNR values of all the electrodes used are displayed in Table 4-2 using Equation 4-1. Considering the margin of error, the highest SNR obtained was for the extrusion printed square, and the lowest was for the inkjet printed spiral matrix. Given the lower sheet resistance of the extrusion printed electrodes and the larger contact areas of the square, the extrusion printed square would possess a higher SNR. Conversely, the inkjet printed square would have a lower SNR due to a significantly smaller contact area and higher sheet resistance. T-tests were conducted to determine whether any of the resulting SNR values were statistically different from one another. There was no significant difference in SNR between EX Square (M = 28.46, SD = 2.14) and IJ Square (M = 26.79, SD = 6.65); t(6) = [-0.14], p = [0.90]. The p-values comparing the extrusion and inkjet printed squares to the conventional electrode were both 0.85. In all cases,

the p-values were greater than the set value for α (0.05), indicating a lack of statistically significant differences.

As shown in Figure *4-8*a, the inkjet printed square had large peaks at the start and end of the muscle signal and fairly low noise present between contractions. This resulted in a higher SNR compared to the other shapes printed with the same method. It is also notable that the extrusion printed spiral matrix possessed a higher SNR than the extrusion printed circle, but the opposite was the case for the inkjet printed shapes. Since the inkjet printed patterns were more susceptible to breaks due to the presence of pores in the tattoo paper, a pattern with thin lines would potentially have disconnections. The extrusion printing process of circles resulted in a partial gap between the outline and inner part of the circle, resulting in a disconnect. This issue can be addressed with further optimization of the extrusion printer g-code.

Table 4-2. SNR Results of EMG signals obtained with conventional, inkjet printed tattoo, and extrusion printed tattoo electrodes. IJ denotes inkjet printed and EX denotes extrusion printed.

Electrode type	**SNR (dB)**	**Electrode type**	**SNR (dB)**
Conventional	25.96 ± 2.36	EX Square	28.46 ± 2.14
IJ Square	26.79± 6.65	EX Circle	19.78 ± 3.77
IJ Circle	11.31 ± 2.29	EX Spiral matrix	26.27 ± 1.87
IJ Spiral matrix	7.93 ± 2.25		

Comparisons of the tattoos presented in this work to medical tattoos in the literature can be seen in Table 4-3. The silver medical electrodes from this work possessed a generally higher SNR (calculated using both formulas mentioned) compared to the tattoos developed with organic materials. This can be attributed to the more electrically robust nature of the silver material used.

Table 4-3. SNR values for this work and select literature sources. Values with * are calculated with Equation 4-2, all others are calculated with Equation 4-1.

Tattoo electrode material	**Fabrication method**	**Biomedical signals acquired**	**Approximate SNR (dB)**
Graphene [9]	CVD and cutting	ECG	15
Carbon/ppEDOT [30]	Screen printing	sEMG	22
PEDOT:PSS [23]	Inkjet printing	EMG	11
PEDOT:PSS [62]	Gravure printing	sEMG	37*
Silver nanoparticle square	Inkjet printing	EMG	26.79 ± 6.65, 35.83 ± 1.57*
Silver flake square	Extrusion printing	EMG	28.46 ± 2.14, 37.80 ± 2.23*

4.4. Impedance Tests

Additional impedance tests of the electrodes were also done on a human subject (see Figure 4-10). The impedance over contact area was also plotted, as shown in Figure 4-10, to show a more clear comparison of the impedance when taking the surface area of the electrode into account. In the latter plot, the extrusion printed square possessed a lower impedance compared to the conventional and inkjet printed tattoo electrode. This was in line with the previous impedance results acquired with the phantom model.

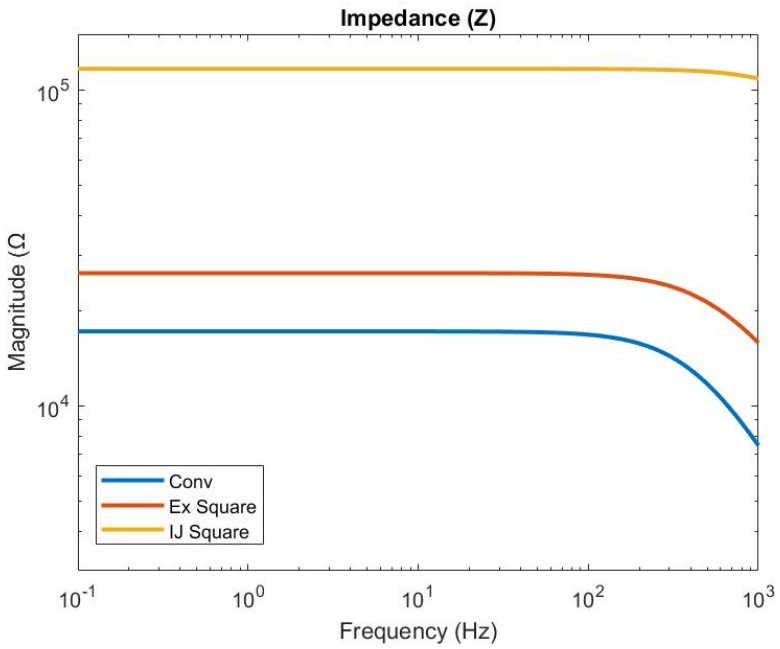

Figure 4-9. Human impedance results with conventional, inkjet (IJ) printed square, and extrusion (Ex) printed square electrodes

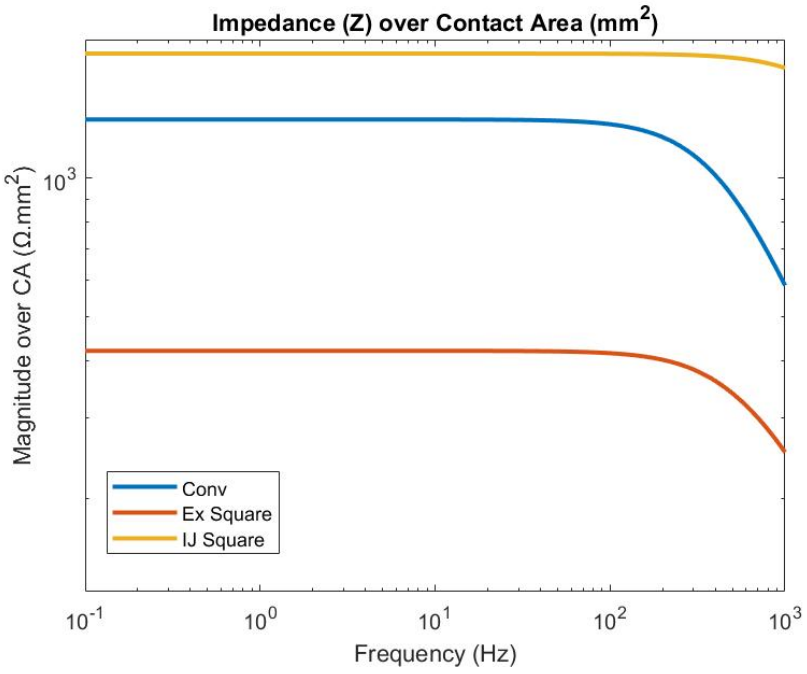

Figure 4-10. Human impedance results with conventional, inkjet (IJ) printed square, and extrusion (Ex) printed square electrodes over contact area

A summary of the impedances from this work and literature sources can be seen in Table 4-4. Revisiting the previous impedances from the literature, the impedance of the graphene-based tattoos from [9] was comparable to their conventional counterpart, but their size was 10 times smaller (24.5 mm^2), essentially making their impedance one order of magnitude smaller. Another example from [30] showed that the screen printed carbon/ppEDOT tattoo array had an impedance approximately one order of magnitude higher than the reference Ag/AgCl electrode, but was 15 times smaller in terms of surface area (at 20 mm^2), making their impedance slightly lower. The printed PEDOT:PSS tattoos from [23] showed a significantly larger impedance compared to their conventional counterpart, even with a larger contact area (at 100 mm^2). In comparison, the impedance in the lower frequency range for both the inkjet and extrusion printed tattoo electrodes are lower than the values presented in the literature and would be further reduced due to their size.

Table 4-4. Impedance over contact area for this work and select literature sources

Tattoo electrode material	**Contact area (mm^2)**	**Approximate impedance range**
Graphene [9]	24.5	200k @ 0.1 Hz to 20k @ 2000 Hz
Carbon/ppEDOT [30]	20	600k @ 30 Hz to 20k @ 3000 Hz
PEDOT:PSS [23]	100	8M @ 0.1 Hz to 200k @ 1000 Hz
Silver nanoparticle	16	100k @ 0.1 Hz to 80k @ 3000 Hz
Silver flake	16	20k @ 0.1 Hz to 8k @ 3000 Hz

4.5. Conclusion

The inkjet and extrusion printed tattoo electrodes were implemented in the acquisition of biophysical (ECG and EMG) signals. The different shapes printed using each method were compared in terms of visual and electrical quality. In terms of signal appearance, there was no notable difference in the ECG signals acquired with the inkjet and extrusion printed electrodes, however the extrusion printed electrodes outperformed the inkjet printed electrodes when used to

record EMG signals. Upon analysis, the extrusion printed square electrode showed a better performance compared to the other electrodes in terms of signal definition. In terms of SNR, the values acquired for the conventional and tattoo electrodes showed no statistically significant difference, indicating that the tattoo electrodes perform just as well as the gold-standard electrode.

CHAPTER 5. CONCLUSION AND FUTURE WORK

5.1. Conclusions

In this thesis, the fabrication, in vitro testing, and in vivo implementation of novel printed silver-based medical tattoo electrodes is presented. The tattoo electrodes serve as a thinner, flexible, and more robust alternative to conventional medical tattoos used for biophysical signal acquisition. Optimization of the fabrication of medical tattoo electrodes opens the door for further development of tattoo-based medical sensors and devices developed using printing-based methods.

In chapter 2, the fabrication process of the medical tattoo electrodes using inkjet and extrusion printing methods is discussed. The use of printing methods with inks composed of silver, an electrically and mechanically robust material, demonstrated efficient fabrication and design flexibility of the tattoos. Given the challenge of printing a low viscosity ink on a porous, absorptive substrate during inkjet printing, additional steps, such as printing multiple layers, were taken to optimize the resulting electrode pattern. Conversely, the viscous nature of the silver flake ink used for extrusion printing allowed for the printed pattern to remain intact on the tattoo paper, which simplified the fabrication process.

In chapter 3, in vitro testing of the tattoo electrodes was completed to initially examine their electrical and mechanical behaviour. Vital parameters such as impedance and bending strain were measured to investigate the initial performance of the tattoo electrodes. Impedance tests were conducted with a phantom model, which mimicked the process of the transfer of potentials from an organ (e.g. the heart) to the surface of the skin for measurement. The results of the initial testing showed that the extrusion printed electrodes performed better than the inkjet printed electrodes in terms of impedance and bending.

In chapter 4, the tattoo electrodes were tested on human subjects to examine the effectiveness of the tattoo electrodes toward the acquisition of biophysical signals. ECG and EMG signals using tattoo electrodes of various shapes were acquired from human participants and compared to

conventional medical snap electrodes in terms of signal quality. In terms of SNR, the tattoo and conventional electrodes were statistically similar, indicating that the tattoo electrodes would ultimately be a suitable alternative.

5.2. Future Work

Given the optimization of the inkjet and extrusion printing process of the silver-based inks on the tattoo paper, other ink formulations can potentially be used to print patterns on tattoo paper. Other biocompatible metal-based inks, such as gold, can be used for printing designs on the substrate in discussion. Since there has been no use of extrusion printing on tattoo paper prior to this work, other high-viscosity inks, such as screen-printable PEDOT:PSS inks, can be used.

With the use of printing process to form designs on tattoo paper, more complex patterns can potentially be developed as well. In particular, other components (e.g. RFID tags, strain sensors) can be easily designed and patterned on the tattoo paper. These printing methods can also be used to form circuits to examine biomarkers in a more discreet fashion. For example, a tattoo electrode array with printed wires can directly connect to a small EMG sensor chip with a wireless module on a wearable article (i.e. skin patch, bracelet) to acquire and transmit EMG signals from a limb on the body.

The acquisition of other mechanical parameters, such as strain, would also be an important aspect to study as the surface that the tattoo ultimately sits on (skin) is consistently subjected to it. The tattoo can be applied onto a flexible substrate, such as PDMS, and be subjected to varying degrees of tensile stress to examine the change in resistance, similarly to the bending tests.

A significant aspect of the medical tattoo electrodes that was discussed but not explored in this work was the long-term use of the tattoos. It would be insightful to examine the long-term usage of the tattoos and see how well the signals remain intact over the course of several hours/days. Since previous works have found that tattoo electrodes improve in performance over

time due to the accumulation of sweat facilitating ionic conductivity at the surface of the skin, it would be interesting to see how the silver tattoo electrodes fare in comparison. The performance of the electrodes during and after physical activity would also be a useful aspect to study further.

REFERENCES

[1] Neuman, M. R. “Biopotential Electrodes.” The Biomedical Engineering Handbook: Second Edition. Ed. Joseph D. Bronzino Boca Raton: CRC Press LLC, 2000

[2] Sbszipper, “The classification of Metal Button Manufacturing Process,” *Decorative Zips and Fashion Trend*, 08-Apr-2019. [Online]. Available: https://www.sbs-zipper.com/blog/the-classification-of-metal-button-manufacturing-process/. [Accessed: 04-Jul-2022].

[3] J. V. Cartmell, M. L. Wolf, and W. Sturtevant, “METHOD OF MANUFACTURING A DISPOSABLE ELECTRODE,” 13-Jun-2000.

[4] Q. Li, J. Zhang, Q. Li, G. Li, X. Tian, Z. Luo, F. Qiao, X. Wu, and J. Zhang, “Review of printed electrodes for flexible devices,” *Frontiers in Materials*, vol. 5, 2019.

[5] M. Hambsch, K. Reuter, M. Stanel, G. Schmidt, H. Kempa, U. Fügmann, U. Hahn, and A. C. Hübler, “Uniformity of fully gravure printed organic field-effect transistors,” *Materials Science and Engineering: B*, vol. 170, no. 1-3, pp. 93–98, 2010.

[6] X. Xu, M. Luo, P. He, and J. Yang, “Washable and flexible screen printed graphene electrode on textiles for Wearable Healthcare Monitoring,” *Journal of Physics D: Applied Physics*, vol. 53, no. 12, p. 125402, 2020.

[7] Lo, J., Lee, DJL, Wong, N., Bui, D., & Paulos, E. (2016). Skintillates: Designing and creating epidermal interactions. UC Berkeley. http://dx.doi.org/10.1145/2901790.2901885 Retrieved from https://escholarship.org/uc/item/4pc7k9gh

[8] Ferrari, Laura M., Usein Ismailov, Jean-Michel Badier, Francesco Greco, and Esma Ismailova. “Conducting Polymer Tattoo Electrodes in Clinical Electro- and Magneto-Encephalography.” Npj Flexible Electronics 4, no. 1 (March 17, 2020): 1–9. https://doi.org/10.1038/s41528-020-0067-z.

[9] Kabiri Ameri, Shideh, Rebecca Ho, Hongwoo Jang, Li Tao, Youhua Wang, Liu Wang, David M. Schnyer, Deji Akinwande, and Nanshu Lu. “Graphene Electronic Tattoo Sensors.” ACS Nano 11, no. 8 (August 22, 2017): 7634–41. https://doi.org/10.1021/acsnano.7b02182.

[10] L. M. Ferrari, K. Keller, B. Burtscher, and F. Greco, “Temporary tattoo as unconventional substrate for conformable and transferable electronics on skin and beyond,” *Multifunctional Materials*, vol. 3, no. 3, p. 032003, 2020.

[11] I. J. Fernandes, A. F. Aroche, A. Schuck, P. Lamberty, C. R. Peter, W. Hasenkamp, and T. L. Rocha, “Silver nanoparticle conductive inks: Synthesis, characterization, and fabrication of inkjet-printed flexible electrodes,” *Scientific Reports*, vol. 10, no. 1, 2020.

[12] “Top 10 thermally conductive materials,” *Thermtest Inc.*, 02-Jun-2021. [Online]. Available: https://thermtest.com/thermal-resources/top-10-thermally-conductive-materials#:~:text=Silver%20%E2%80%93%20429%20W%2Fm%E2%80%A2K.

[13] N. Ibrahim, J. O. Akindoyo, and M. Mariatti, “Recent development in silver-based ink for flexible electronics,” *Journal of Science: Advanced Materials and Devices*, vol. 7, no. 1, p. 100395, 2022.

[14] Y. Meng and J. D. Mackenzie, “Highly conductive silver flake/nanowire composites inks and 3D printing processing in flexible electrodes application,” thesis.

[15] “Graphene - what is it?,” *Graphenea*. [Online]. Available: https://www.graphenea.com/pages/graphene#.YsIaM3bMI2w. [Accessed: 04-Jul-2022].

[16] “Graphene inks for printed electronics,” *Sigma Aldrich*. [Online]. Available: https://www.sigmaaldrich.com/CA/en/technical-documents/technical-article/materials-science-and-engineering/3d-printing/graphene-inks-for-printed-electronics. [Accessed: 04-Jul-2022].

[17] “PEDOT:PSS: PH1000, AI4083, HTL Solar & HTL Solar 3, F HC solar,” *Ossila*. [Online]. Available: https://www.ossila.com/en-ca/products/pedot-pss. [Accessed: 04-Jul-2022].

[18] “Inkjet Printing and patterning of Pedot-PSS: Application to optoelectronic devices,” *Conjugated Polymers*, pp. 165–186, 2006.

[19] I. Basak, G. Nowicki, B. Ruttens, D. Desta, J. Prooth, M. Jose, S. Nagels, H.-G. Boyen, J. D'Haen, M. Buntinx, and W. Deferme, "Inkjet printing of Pedot:PSS based conductive patterns for 3D forming applications," *Polymers*, vol. 12, no. 12, p. 2915, 2020.

[20] K. Alaqad and T. A. Saleh, "Gold and silver nanoparticles: Synthesis methods, characterization routes and applications towards drugs," *Journal of Environmental & Analytical Toxicology*, vol. 6, no. 4, 2016.

[21] H. R. Tiyyagura, P. Majerič, M. Bračič, I. Anžel, and R. Rudolf, "Gold inks for inkjet printing on photo paper: Complementary characterisation," *Nanomaterials*, vol. 11, no. 3, p. 599, 2021.

[22] *Ink-Jet Microdispensing Basic Set-up*, 1st ed. MicroFab Technologies, Inc., Plano, TX, 2012.

[23] E. Bihar *et al.*, "Fully printed all-polymer tattoo/textile electronics for electromyography," *Flex. Print. Electron.*, vol. 3, no. 3, p. 034004, Sep. 2018, doi: 10.1088/2058-8585/aadb56.

[24] A. A. Chlaihawi, B. B. Narakathu, S. Emamian, B. J. Bazuin, and M. Z. Atashbar, "Development of printed and flexible dry ECG electrodes," Sensing and Bio-Sensing Research, vol. 20, pp. 9–15, Sep. 2018, doi: 10.1016/j.sbsr.2018.05.001.

[25] J. Yoo, L. Yan, S. Lee, H. Kim, and H.-J. Yoo, "A Wearable ECG Acquisition System With Compact Planar-Fashionable Circuit Board-Based Shirt," IEEE Transactions on Information Technology in Biomedicine, vol. 13, no. 6, pp. 897–902, Nov. 2009, doi: 10.1109/TITB.2009.2033053.

[26] H. Jin, N. Matsuhisa, S. Lee, M. Abbas, T. Yokota, and T. Someya, "Enhancing the Performance of Stretchable Conductors for E-Textiles by Controlled Ink Permeation," Advanced Materials, vol. 29, no. 21, p. 1605848, 2017, doi: 10.1002/adma.201605848.

[27] R. G. Scalisi et al., "Inkjet printed flexible electrodes for surface electromyography," Organic Electronics, vol. 18, pp. 89–94, Mar. 2015, doi: 10.1016/j.orgel.2014.12.017.

[28] S. Wang, J. Yan, C. Zhu, J. Yao, Q. Liu, and X. Yang, “A Low Contact Impedance Medical Flexible Electrode Based on a Pyramid Array Micro-Structure,” Micromachines (Basel), vol. 11, no. 1, p. 57, Jan. 2020, doi: 10.3390/mi11010057.

[29] S. Taccola et al., “Toward the Use of Temporary Tattoo Electrodes for Impedancemetric Respiration Monitoring and Other Electrophysiological Recordings on Skin,” Sensors, vol. 21, no. 4, Art. no. 4, Jan. 2021, doi: 10.3390/s21041197.

[30] L. Bareket et al., “Temporary-tattoo for long-term high fidelity biopotential recordings,” Sci Rep, vol. 6, no. 1, Art. no. 1, May 2016, doi: 10.1038/srep25727.

[31] V. K. Rao R, V. Abhinav K, K. P. S, and S. Prakash Singh, “Conductive silver inks and their applications in printed and flexible electronics,” RSC Advances, vol. 5, no. 95, pp. 77760–77790, 2015, doi: 10.1039/C5RA12013F.

[32] I. J. Fernandes et al., “Silver nanoparticle conductive inks: synthesis, characterization, and fabrication of inkjet-printed flexible electrodes,” Sci Rep, vol. 10, no. 1, Art. no. 1, Jun. 2020, doi: 10.1038/s41598-020-65698-3.

[33] G. Cho, K. Jeong, M. J. Paik, Y. Kwun, and M. Sung, “Performance Evaluation of Textile-Based Electrodes and Motion Sensors for Smart Clothing,” IEEE Sensors Journal, vol. 11, no. 12, pp. 3183–3193, Dec. 2011, doi: 10.1109/JSEN.2011.2167508.

[34] J. Alberto et al., “Fully Untethered Battery-free Biomonitoring Electronic Tattoo with Wireless Energy Harvesting,” Sci Rep, vol. 10, no. 1, p. 5539, Dec. 2020, doi: 10.1038/s41598-020-62097-6.

[35] K. S. Cole and R. H. Cole, “Dispersion and Absorption in Dielectrics I. Alternating Current Characteristics,” J. Chem. Phys., vol. 9, no. 4, pp. 341–351, Apr. 1941, doi: 10.1063/1.1750906.

[36] S. Grimnes and Ø. G. Martinsen, “Chapter 7 - Electrodes,” in Bioimpedance and Bioelectricity Basics (Third Edition), S. Grimnes and Ø. G. Martinsen, Eds. Oxford: Academic Press, 2015, pp. 179–254. doi: 10.1016/B978-0-12-411470-8.00007-6.

[37] Leleux P, Rivnay J, Lonjaret T, Badier J-M, B´enar C, Herv´e T, Chauvel P and Malliaras G G 2015 Organic electrochemical transistors for clinical applications Adv. Healthcare Mater. 4 142–7

[38] Keller P E and Kouzes R T 2017 Water vapor permeation in plastics [Internet]. Jan p PNNL–26070, 1411940. Report No.: PNNL–26070, 1411940

[39] McKeen L 2017 Permeability Properties of Plastics and Elastomers Fourth edn (Amsterdam, Boston: Elsevier William Andrew) pp 359

[40] M. S. Rahman and G. Grau, "Direct writing of stretchable metal flake conductors: improved stretchability and conductivity by combining differently sintered materials," Flex. Print. Electron., vol. 5, no. 2, p. 025005, Jun. 2020, doi: 10.1088/2058-8585/ab8f22.

[41] M. S. Rahman, M. Shahzadeh, M. Rahman, S. Pisana, and G. Grau, "High-speed contactless sintering characterization for printed electronics by frequency-domain thermoreflectance," Flex. Print. Electron., vol. 5, no. 3, p. 035006, Aug. 2020, doi: 10.1088/2058-8585/aba8ea.

[42] J. S. Kang, J. Ryu, H. S. Kim, and H. T. Hahn, "Sintering of Inkjet-Printed Silver Nanoparticles at Room Temperature Using Intense Pulsed Light," J. Electron. Mater., vol. 40, no. 11, p. 2268, Aug. 2011, doi: 10.1007/s11664-011-1711-0.

[43] D. Mitra, K. Y. Mitra, M. Hartwig, and R. R. Baumann, "Intense Pulsed Light Sintering of an Inkjet Printed Silver Nanoparticle Ink Depending on the Spectral Absorption and Reflection of the Background," jist, vol. 60, no. 4, pp. 40403-1-40403–5, Jul. 2016, doi: 10.2352/J.ImagingSci.Technol.2016.60.4.040403.

[44] "Binder - PrintWiki." http://printwiki.org/Binder (accessed Aug. 02, 2022).

[45] O.-H. Huttunen, M. H. Behfar, J. Hiitola-Keinänen, and J. Hiltunen, "Electronic Tattoo with Transferable Printed Electrodes and Interconnects for Wireless Electrophysiology Monitoring," Advanced Materials Technologies, vol. n/a, no. n/a, p. 2101496, doi: 10.1002/admt.202101496.

[46] G. Grau, R. Kitsomboonloha, S. L. Swisher, H. Kang, and V. Subramanian, "Printed Transistors on Paper: Towards Smart Consumer Product Packaging," Advanced Functional Materials, vol. 24, no. 32, pp. 5067–5074, 2014, doi: 10.1002/adfm.201400129.

[47] L. J. Van Der Pauw, "A Method of Measuring Specific Resistivity and Hall Effect of Discs of Arbitrary Shape." Philips Research Reports 12.1 (1958): 1-9. Print

[48] A. Y. Owda and A. J. Casson, "Electrical properties, accuracy, and multi-day performance of gelatine phantoms for electrophysiology." bioRxiv, p. 2020.05.30.125070, May 31, 2020. doi: 10.1101/2020.05.30.125070.

[49] C.-C. Huang, S.-H. Hung, J.-F. Chung, L.-D. Van, and C.-T. Lin, *Front-end amplifier of low-noise and tunable BW/gain for portable biomedical signal acquisition*. 2008, p. 2720. doi: 10.1109/ISCAS.2008.4542018.

[50] M. N. Maghribi, P. A. Krulevitch, T. S. Wilson, J. K. Hamilton, and C. Park, "Serpentine and corduroy circuits to enhance the stretchablity of a stretchable electronic device," WO2004107973A1, Dec. 16, 2004 Accessed: Jul. 24, 2022. [Online]. Available: https://patents.google.com/patent/WO2004107973A1/zh

[51] "Electrocardiogram (ECG or EKG) - Mayo Clinic." https://www.mayoclinic.org/tests-procedures/ekg/about/pac-20384983

[52] "The ECG Leads, Polarity and Einthoven's Triangle," The Student Physiologist, Oct. 20, 2015. https://thephysiologist.org/study-materials/the-ecg-leads-polarity-and-einthovens-triangle/

[53] S. S. Barold, "Willem Einthoven and the Birth of Clinical Electrocardiography a Hundred Years Ago," Card Electrophysiol Rev, vol. 7, no. 1, pp. 99–104, Jan. 2003, doi: 10.1023/A:1023667812925.

[54] E. A. Ashley and J. Niebauer, Conquering the ECG. Remedica, 2004. Accessed: Aug. 08, 2022. [Online]. Available: https://www.ncbi.nlm.nih.gov/books/NBK2214/

[55] A. J. Moss, “Gender Differences in ECG Parameters and Their Clinical Implications,” Ann Noninvasive Electrocardiol, vol. 15, no. 1, pp. 1–2, Jan. 2010, doi: 10.1111/j.1542-474X.2009.00345.x.

[56] “Signal-to-noise ratio - MATLAB snr.” https://www.mathworks.com/help/signal/ref/snr.html (accessed Aug. 15, 2022).

[57] “Butterworth filter design - MATLAB butter.” https://www.mathworks.com/help/signal/ref/butter.html (accessed Aug. 08, 2022).

[58] B. Salsekar and D. Wadhwani, “Filtering of ECG signal using Butterworth Filter and its feature extraction,” International Journal of Engineering Science and Technology, vol. 4, Apr. 2012.

[59] K. K. Fu, Z. Wang, J. Dai, M. Carter, and L. Hu, “Transient Electronics: Materials and Devices,” Chem. Mater., vol. 28, no. 11, pp. 3527–3539, Jun. 2016, doi: 10.1021/acs.chemmater.5b04931.

[60] S. K. Ameri, N. Lu, and D. Akinwande, “(Invited) Imperceptible Graphene Based Electronic Tattoo Sensors,” Meet. Abstr., vol. MA2018-01, no. 26, p. 1535, Apr. 2018, doi: 10.1149/MA2018-01/26/1535.

[61] J. R. Windmiller, A. J. Bandodkar, G. Valdés-Ramírez, S. Parkhomovsky, A. G. Martinez, and J. Wang, “Electrochemical sensing based on printable temporary transfer tattoos,” Chem. Commun., vol. 48, no. 54, p. 6794, 2012, doi: 10.1039/c2cc32839a.

[62] A. Zucca et al., “Tattoo Conductive Polymer Nanosheets for Skin-Contact Applications,” Advanced Healthcare Materials, vol. 4, no. 7, pp. 983–990, 2015, doi: 10.1002/adhm.201400761.

[63] A. Spanu et al., “Parylene C-Based, Breathable Tattoo Electrodes for High-Quality Bio-Potential Measurements,” Frontiers in Bioengineering and Biotechnology, vol. 10, 2022, Accessed: Aug. 17, 2022. [Online]. Available: https://www.frontiersin.org/articles/10.3389/fbioe.2022.820217

[64] T. Ha et al., “A Chest-Laminated Ultrathin and Stretchable E-Tattoo for the Measurement of Electrocardiogram, Seismocardiogram, and Cardiac Time Intervals,” Advanced Science, vol. 6, no. 14, p. 1900290, 2019, doi: 10.1002/advs.201900290.

[65] A. J. Bandodkar, W. Jia, C. Yardımcı, X. Wang, J. Ramirez, and J. Wang, “Tattoo-Based Noninvasive Glucose Monitoring: A Proof-of-Concept Study,” Anal. Chem., vol. 87, no. 1, pp. 394–398, Jan. 2015, doi: 10.1021/ac504300n.

[66] N. X. Williams and A. D. Franklin, “Electronic Tattoos: A Promising Approach to Real-time Theragnostics,” Journal of Dermatology and Skin Science, vol. 2, no. 1, Mar. 2020, Accessed: Aug. 17, 2022. [Online]. Available: https://www.dermatoljournal.com/articles/electronic-tattoos-a-promising-approach-to-real-time-theragnostics.html

[67] A. Pepłowski, D. Janczak, P. Krzemińska, and M. Jakubowska, “Temporary tattoo for wireless human pulse measurement,” in Photonics Applications in Astronomy, Communications, Industry, and High-Energy Physics Experiments 2016, Sep. 2016, vol. 10031, pp. 701–708. doi: 10.1117/12.2248211.

[68] “Electromyography (EMG) - Mayo Clinic.” https://www.mayoclinic.org/tests-procedures/emg/about/pac-20393913 (accessed Aug. 25, 2022).

[69] F. H. A. Salem, K. S. Mohamed, S. B. K. Mohamed, and A. A. El Gehani, “The Development of Body-Powered Prosthetic Hand Controlled by EMG Signals Using DSP Processor with Virtual Prosthesis Implementation,” Conference Papers in Engineering, vol. 2013, p. e598945, Jun. 2013, doi: 10.1155/2013/598945.